Thermophoresis of a spherical particle in a permeable microchannel with thermal stress slip

M. S. Faltas,[1] H. H. Sherief,[1] Allam A. Allam,[2] M. G. Nashwan,[1] and M. El-Sayed[2,*]

[1]*Department of Mathematics, Faculty of Science, Alexandria University, Alexandria 21568, Egypt*

[2]*Institute of Basic and Applied Science, College of Engineering and Technology, Arab Academy for Science, Technology and Maritime Transport, Alexandria 21937, Egypt*

(Received 22 October 2022; accepted 13 April 2023; published 12 May 2023)

The quasisteady thermophoretic motion of a spherical aerosol particle situated at an arbitrary position in a microchannel with naturally permeable plane walls bounding a porous medium is studied semianalytically. The applied temperature gradient is constant and perpendicular to the walls of the channel. The appropriate field equations of energy and momentum for the system are solved using a boundary collocation technique in the limit of small Péclet and Reynolds numbers. The effect of thermal stress slip at the surface of the particle is included in this paper in addition to temperature jump, thermal creep, and frictional slip. This paper is motivated by a wide variety of flows such as the deposit of particles in reverse osmosis processes, dialysis, or various biological organs where fluid passes through membranes or cell walls. The collocation results of the normalized thermophoretic velocity are obtained with adequate accuracy for a wide range of values of the relative thermal conductivity, permeability of the walls, and surface properties of the particle. Thermophoretic velocity is also obtained for the particular case of the migration of a spherical particle in an unbounded fluid medium in the presence of a single permeable plane surface and it is found in perfect agreement with the corresponding data available in the literature. The normalized thermophoretic velocity of the confined particle decreases significantly when the particle is in near contact with the microchannel walls. It decreases also as the permeability parameter of the walls increases. It is also found that the thermal stress slip coefficient has a significant rule on the normalized thermophoretic velocity.

DOI: 10.1103/PhysRevFluids.8.054102

I. INTRODUCTION

When a solid particle is immersed in a fluid holding a temperature gradient, it gains a velocity relative to the fluid in the direction of decreasing temperature. This anomaly, known as thermophoresis, was discovered by Tyndall [1]. Therefore, thermophoresis is a mechanism for the trapping of aerosol particles on cool surfaces [2–7]. Thermophoresis has a wide range of practical applications such as aerosol sampling, air cleaning, microelectronic manufacturing, scale formation on heat exchanger surfaces, removal of soot particles for combustion exhaust gas systems, modified chemical vapor deposition, and nuclear reactor safety [8–12].

In the present paper, it is relevant to define the Knudsen number (Kn). This number relates the molecular mean-free path ℓ of gas to the radius a of an aerosol particle, i.e., $\mathrm{Kn} = \ell/a$. For continuum flows, the Knudsen number is very small ($\mathrm{Kn} \ll 1$), the flow is known as the hydrodynamic regime, and obeys the Navier-Stokes equation. In fact, the appropriate flow and heat transfer models depend on the range of the Knudsen number. A categorization of the various

*Corresponding author: m.elsayed97@egypt.aast.edu

flow regimes is given as follows: (i) slip flow regime, $0.01 < \mathrm{Kn} < 0.1$, (ii) transitional regime, $0.1 < \mathrm{Kn} < 10$, and (iii) free molecular regime, $\mathrm{Kn} > 10$. In the slip flow regime, the velocity slip and the temperature jump phenomena appear at the boundaries immersed in the flow [13,14]. Therefore, in the next analysis, we employ the continuum with slippage approach. This requires using the Stokes-Navier model and, in this case, the Knudsen number should be smaller than about 0.1.

The thermophoresis motion of isolated particles is treated extensively in the literature under the assumptions of vanishingly small Péclet and Reynolds numbers with different physical circumstances, e.g., Refs. [15–18]. Fayolle *et al.* [19] studied the thermally induced particle flow in a charged colloidal suspension in a fluid-mechanical approach. The authors obtained the drift velocity and the thermophoretic transport coefficients and compared their results with the available data in the literature. Morthomas and Würger [20] found the thermophoretic mobility of charged particles as a function of the Navier slip length b. One of their findings is that if b exceeds the particle size a, the enhancement coefficient a/λ is independent of b but proportional to the particle size, where λ is the Debye length. Würger [21] used a hydrodynamic approach to investigate the thermophoretic transport in colloidal suspensions, with slippage imposed by thermal Marangoni forces. The author concluded that the thermophoresis due to surface forces is insensitive to hydrodynamic interactions and the thermal diffusion coefficient of polymer solutions is independent of molecular weight and concentration. An interesting theoretical investigation was addressed by Ly and Würger [22] for the molecular-weight dependence of DNA thermophoresis which arises from the mutual advection of the n repeat units of the molecular chain. Duhr *et al.* [23] addressed the Thermophoresis problem of DNA determined by microfluidic fluorescence. Parola and Piazza [24] presented a microscopic description of thermophoretic phenomena in dilute suspensions of spherical colloids. The authors found a general expression for the Soret coefficient and applied it to the specific cases of neutral colloids in pure solvent and of Debye-Hückel systems. Padrino *et al.* [25] modeled the slow thermophoresis, steady gas dynamics surrounding a rigid, heat-conducting spherical particle using the linearized form of the regularized 13-moment equations (R13) in the presence of a uniform temperature gradient in the far field. Many authors performed experimental work on the applications of thermophoresis in different branches of science, e.g., Refs. [26–33]. In addition to the thermal creep, another velocity slip acted at the surface of the particle, called thermal stress slip, was suggested by Sone [34]. It results from the variation of the fluid temperature in tangential and normal directions [35]. Many authors included the thermal stress slip in their studies, e.g., Refs. [36–41]. They found that the effects of thermal stress slip can be significant when the Knudsen number is not too small or the particle is not too large. However, in most real applications of thermophoresis, aerosol particles are confined by solid or permeable walls. The dimensions of the aerosol particles and bounding microchannels are comparable, and it is required to find out if the closeness of the channel wall significantly affects the particle velocity [42–46].

A wide range of studies have been found in the literature on the flows where particles interact with naturally permeable boundaries, e.g., filter beds in water purification plants, the deposit of particles in reverse osmosis processes, and dialysis or various biological organs where fluid passes through cell walls. Using bispherical coordinates, O'Neill and Bhatt [47] obtained exact solutions for the motion of a spherical particle embedded in a Newtonian fluid bounded by a naturally permeable plane surface. Würger [48] considered the hydrodynamic problem of slowing a particle moving through a temperature gradient perpendicular to a wall at distances much smaller than the particle radius. The author found that the trapping efficiency, or effective Soret coefficient, increases logarithmically as the particle gets very close to the wall. His results provide a quantitative explanation for the recently observed enhancement of thermophoretic trapping at short distances. Damiano *et al.* [49] modeled a biological system as a spherical particle embedded in a Stokes flow bounding a Brinkman half space. The authors considered the parallel motion to the bounding plane and found solutions for small values of the dimensionless hydraulic permeability of the Brinkman medium. Recently, Faltas *et al.* [50] studied the isothermal axisymmetric motion of a slip spherical particle in the presence of a porous interface. The authors modeled the flow through the porous

medium using Brinkman equation [51] with a tangential stress jump at the bounding plane surface [52,53]. They found that the porous bounding surface has a significant effect on the drag force acting on the particle.

In this paper, we provide the semianalytical solution to the axisymmetric thermophoretic motion of an aerosol spherical particle at an arbitrary position in a permeable microchannel filled with Newtonian fluid. The flow region outside the microchannel is governed by Darcy's equation. The microchannel walls are prescribed with a linear temperature distribution. The temperature jump, frictional slip, thermal creep, and thermal stress slip effects at the solid surface of the particle are included. The appropriate hydrodynamic and energy equations are solved using the boundary collocation method, and the thermophoretic mobility of the confined particle is determined as a function of the permeability of the microchannel and the other relevant parameters.

II. HEAT ENERGY AND MOMENTUM EQUATIONS

The governing equations that model an incompressible Newtonian fluid flow in the absence of external body forces are [54]

$$\nabla \cdot \vec{u} = 0, \tag{2.1}$$

$$\rho_f \left(\frac{\partial \vec{u}}{\partial t} + \vec{u} \cdot \nabla \vec{u} \right) = -\nabla p + \mu \nabla^2 \vec{u}, \tag{2.2}$$

and the equation that models the heat transfer in a fluid is

$$\frac{\partial T}{\partial t} + \vec{u} \cdot \nabla T = \frac{k}{\rho_f c_p} \nabla^2 T, \tag{2.3}$$

where $\vec{u}, T, p$ are, respectively, the velocity, pressure, and temperature. Here the constants (ρ_f, μ, k, c_p) are, respectively, the density, viscosity coefficient, thermal conductivity, and specific heat. The constitutive equations of the flow are

$$\Pi = -pI + \mu(\nabla \vec{u} + \nabla^* \vec{u}), \tag{2.4}$$

$$\vec{q} = -k \nabla T, \tag{2.5}$$

where Π is the stress tensor, $\vec{q}$ is the heat flux vector, I is a unit dyadic, and $(.)^*$ refers to a transpose of a dyadic.

III. DESCRIPTION AND ASSUMPTIONS OF THE PROBLEM

Consider the quasisteady axially symmetric thermophoresis motion of a spherical particle of radius a situated at an arbitrary position in a naturally permeable microchannel filled with a gaseous medium. The microchannel is bounded from the outside by a porous medium of small permeability K. The particle translates perpendicularly to the walls of the microchannel and its center is distant apart z_1 and z_2 from the lower and upper walls of the channel, respectively, as shown in Fig. 1. Let (ρ, ϕ, z) and (r, θ, ϕ) denote the circular cylindrical and spherical coordinate systems, respectively, and the origin of coordinates be chosen at the particle center. The corresponding unit vectors of the two systems are, respectively, $(\vec{e}_\rho, \vec{e}_\phi, \vec{e}_z)$ and $(\vec{e}_r, \vec{e}_\theta, \vec{e}_\phi)$. Far from the particle, a uniform thermal gradient $-E_\infty \vec{e}_z = \nabla T_\infty$, $(E_\infty > 0)$ is imposed on the system. We assume that the Knudsen number Kn is small (Kn < 0.01) so the fluid flow is in the continuum assumption and the Knudsen layer at the particle surface is thin in comparison with the radius of the particle and the spacing between the particle and each wall of the microchannel. Actually, the subsequent analysis can be used also in the slip regime ($0.01 <$ Kn < 0.1) provided that slip boundary conditions are incorporated. Therefore, the Knudsen number Kn of the system should be smaller than about 0.1 to cover the continuum approach with slippage analysis. This means our analysis is valid for aerosol particles (i.e., to the slip

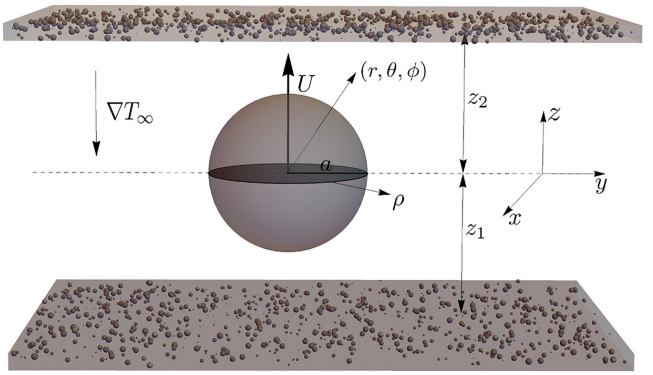

FIG. 1. Geometrical sketch for thermophoresis of a spherical particle perpendicular to permeable plane walls of a microchannel with origin at the particle's center. z_1 and z_2 are, respectively, the distances apart from the center to the lower and upper walls.

regime) and for a standard hydrodynamic regime with an appropriate choice of boundary condition. The aim of this paper is to find out the effect of permeable walls of the microchannel on particle mobility. To determine the thermophoretic velocity of the particle, it is necessary first to find the temperature inside and outside the particle and fluid velocity distributions.

During any interval of time in which temperature changes in time at any position within a fluid or solid body, the thermal energy flow is known as a transient or unsteady state. In many practical applications of heat transfer under various physical circumstances, after the transient period ended, the steady-state temperature is then established. If changes in external temperatures or internal heat generation changes are too rapid for the steady state of temperatures in space to take place, then the system never reaches a state of unchanging. Therefore, it is realistic to assume a steady-state temperature for the solid particle and the fluid. Also, for the case when the fluid flow is slow and with small aerosol particles, the Reynolds and Péclet numbers are quite small. For such cases, the heat energy transfer between fluid and aerosol particles is mainly through heat conduction, which means neglecting the convective effect [16]. However, for large aerosol particles undergoing thermophoresis in high-temperature gradients, the values of the Péclet number would be of the order 0.1 and the convective heat transfer may not be neglected relative to the conduction in the fluid [55]. Therefore, under the assumptions of steady state and low Reynolds and Péclet numbers, Eqs. (2.2) and (2.3) are reduced to

$$\mu\nabla^2\vec{u} = \nabla p, \quad r \geqslant a, \quad -z_1 \leqslant z \leqslant z_2, \tag{3.1}$$

$$\nabla^2 T = 0, \quad r \geqslant a, \quad -z_1 \leqslant z \leqslant z_2, \tag{3.2}$$

$$\nabla^2 T_p = 0, \quad r \leqslant a, \tag{3.3}$$

where T and T_p are, respectively, the temperatures of the fluid and particle.

IV. PERMEABILITY OF THE MICROCHANNEL WALLS

To understand the concept of interaction between the solid particle and the permeable walls of the microchannel, it is important to consider the surrounding medium of the microchannel is a porous material. We model the porous medium by Darcy's law,

$$\nabla P = -\frac{\mu}{K}\vec{v}, \tag{4.1}$$

where ∇P is the pressure gradient within the porous medium and $\vec{v}$ is the filter velocity. The permeability coefficient K is independent of the nature of the fluid but it depends on the geometry of the medium. Now, we have to find the boundary condition that should be applied to the naturally permeable walls of the microchannel. Beavers and Joseph [56] have shown, experimentally, the no-slip condition to be incorrect at the naturally permeable walls and suggested the following semiempirical slip condition:

$$\frac{\partial u_s}{\partial n} = \frac{\beta}{\sqrt{K}}(u_s - v_s), \tag{4.2}$$

with n and s measuring distance normal and tangential to the plane permeable walls of the microchannel and β denotes a slip parameter that is nondimensional and depends on the structure of the porous medium. A theoretical justification of the law Eq. (4.2) was performed by Saffman [57] for small values of the permeability K by using a boundary layer to match the flows in the Darcy region and the Stokes region. He also shows that for small values of the permeability, $\vec{v} = O(K)$, which can be taken zero ($\vec{v} = 0$). Therefore, for small values of permeability K, the first-order solution for the flow in the Stokes region satisfies

$$u_s = \frac{\sqrt{K}}{\beta}\frac{\partial u_s}{\partial n}, \tag{4.3}$$

at the naturally permeable walls. O'Neill and Bhatt [47] used condition Eq. (4.3) in their study of the slow motion of a solid sphere in the presence of a naturally permeable surface.

V. DISTRIBUTION OF HEAT TRANSFER

To find unique solutions of Laplace's Eqs. (2.3) and (2.4) that govern the temperatures T and T_p, we have to specify the boundary conditions at the surface of the particle and at the permeable walls of the microchannel. As we intend to apply the slip-flow regime, it is necessary to consider the temperature jump condition at the surface of the particle [34],

$$T - T_p = C_t \ell \frac{\partial T}{\partial r}, \quad r = a, \tag{5.1}$$

where C_t is the temperature jump coefficient which is nondimensional and depends on the nature of the fluid and particle. It can be calculated using the Boltzmann equation to a Knudsen layer [58]; its value is estimated as of order unity. The calculation of C_t is important in many engineering applications, e.g., aerothermodynamics of space vehicles, vacuum systems, microelectromechanical systems, and many others. The other matching condition is given by

$$k\frac{\partial T}{\partial r} = k_p \frac{\partial T_p}{\partial r}, \quad r = a, \tag{5.2}$$

where k and k_p are the thermal conductivity of the fluid and particle, respectively. Far from the particle ($r \to \infty$), the temperature of the fluid $T \to T_\infty$, where

$$T_\infty = T_o - E_\infty z. \tag{5.3}$$

At the permeable walls of the microchannel, we have

$$T_\infty = T_o + E_\infty z_1, \quad z = -z_1, \tag{5.4}$$

$$T_\infty = T_o - E_\infty z_2, \quad z = z_2. \tag{5.5}$$

Here, the constant T_o refers to the temperature at the center of the particle or the mean temperature of the fluid in the neighborhood of the particle. The nondimensional parameter $\frac{E_\infty a}{T_o}$ is known as the Epstein number and it is a small number in practice [59]. The solutions of Eqs. (2.3) and (2.4)

satisfying conditions (5.3)–(5.5) are similar to those obtained by Keh and Chang [42] for the case of thermophoresis of an aerosol sphere moving perpendicularly to two impermeable plane walls:

$$T = T_o - E_\infty z + E_\infty \sum_{m=0}^{\infty} R_m R_{1m}(r,\theta), \tag{5.6}$$

$$T_p = T_o + E_\infty \sum_{m=0}^{\infty} S_m S_{1m}(r,\theta), \tag{5.7}$$

where the functions $R_{1m}(r,\theta)$ and $S_{1m}(r,\theta)$ are defined in Appendix A. Applying the boundary conditions Eqs. (5.1) and (5.2) to Eqs. (5.6) and (5.7), we obtain

$$\sum_{m=0}^{\infty}[R_m(R_{1m}(a,\theta) - aC_t^* R_{2m}(a,\theta)) - S_m a^m P_m(\zeta)] = a(1-C_t^*)\zeta, \tag{5.8}$$

$$\sum_{m=0}^{\infty}(R_m R_{2m}(a,\theta) - k^* m S_m a^{m-1} P_m(\zeta)) = \zeta, \tag{5.9}$$

where $k^* = \frac{k_p}{k}$, $C_t^* = \frac{C_t \ell}{a}$, $\zeta = \cos\theta$, and $R_{2m}(r,\theta)$ is defined in Appendix A.

To obtain the final forms of the temperature distributions T and T_p, it remains to calculate the unknown coefficients R_m and S_m. This will be done numerically to a finite number of these coefficients by cutting off the series in Eqs. (5.8) and (5.9) into a finite number of terms, M. To precisely satisfy the conditions Eqs. (5.8) and (5.9) along the whole surface of the particle would require the solution of the infinite series of unknown coefficients R_m and S_m. The techniques of collocations [52,60] oblige the boundary conditions at a finite number of discrete points on the semicircular generating arc of the particle and truncates the infinite series in Eqs. (5.8) and (5.9) into finite ones. That means the spherical boundary of the particle is approximated by satisfying Eqs. (5.8) and (5.9) at M discrete points on its generating arc and the infinite series are cut off after M terms, resulting in a system of $2M$ simultaneous linear algebraic equations. This system of equations can be solved numerically to give the $2M$ unknown coefficients ($R_m,\ S_m,\ m = 0, 1, 2, \ldots, M-1$). The precision of the truncation method can be enhanced to any degree by taking a sufficiently large value of M. Basically, as $M \to \infty$ the truncation error vanishes.

VI. DISTRIBUTION OF VELOCITY COMPONENTS

Since the spherical particle translates perpendicular to the permeable walls of the microchannel, then the fluid motion is axisymmetric, and the velocity components of the fluid can be represented in terms of the Stokes stream function through the relation

$$\vec{u} = -\nabla \wedge \left(\frac{\psi}{\rho}\vec{e}_\phi\right). \tag{6.1}$$

The differential equation satisfied by the stream function is obtained from Eq. (2.2) is

$$E^2(E^2\psi) = 0, \tag{6.2}$$

where $E^2 = \frac{\partial^2}{\partial r^2} + \frac{1-\zeta^2}{r^2}\frac{\partial^2}{\partial \zeta^2}$.

The boundary conditions for the fluid velocity at the particle surface $r = a$ are as follows:

$$u_r = U\cos\theta, \tag{6.3}$$

$$u_\theta + U\sin\theta = \frac{C_m \ell}{\mu}\tau_{r\theta} + \frac{\mu C_s}{\rho_f T_o}\frac{1}{r}\frac{\partial T}{\partial \theta} - \frac{\mu C_m \ell C_h}{\rho_f T_o}\frac{\partial}{\partial r}\left(\frac{1}{r}\frac{\partial T}{\partial \theta}\right), \tag{6.4}$$

where U is the thermophoretic velocity of the particle to be determined, $\tau_{r\theta}$ is the tangential stress along the particle surface, C_m is the frictional slip coefficient, C_s is the thermal creep coefficient,

and C_h is the thermal stress slip coefficient. C_m, C_s, and C_h are all dimensionless of order unity. The second and third terms on the right-hand side of condition Eq. (6.4) can be evaluated using Eq. (5.6) after knowing the coefficients R_m out of collocation techniques. The first term on the right-hand side of condition Eq. (6.4) represents frictional or viscous slip. The second term represents the thermal creep flow that is induced by the longitudinal temperature gradient over the surface of the particle. The third term represents a velocity slip known as the thermal stress slip, which was suggested by Sone [34]. Bakanov [36] studied the problem of the thermophoresis of highly heat-conducting bodies by taking into consideration the effect of the thermal stress slip as one of the refinements. The thermal stress velocity term is not accounted for in the previous studies of the thermophoresis motion of a spherical particle embedded in a microchannel.

The boundary conditions on the naturally permeable plane walls of the microchannel can be obtained from Eq. (4.3) as

$$u_z = 0, \quad \frac{\partial u_\rho}{\partial z} = \lambda' u_\rho, \quad \text{on } z = -z_1, \tag{6.5}$$

$$u_z = 0, \quad \frac{\partial u_\rho}{\partial z} = -\lambda' u_\rho, \quad \text{on } z = z_2, \tag{6.6}$$

where $\lambda' = \beta/\sqrt{K}$ is the slip parameter with dimension $(\text{length})^{-1}$. The limiting cases $\lambda' \to \infty$ and $\lambda' = 0$, correspond, respectively, to the rigid walls and free-surface situations. Note that the slip parameter is taken the same for both walls for simplicity. The condition of no motion far from the particle can be expressed as

$$u_z, u_\rho \to 0, \quad \rho \to \infty. \tag{6.7}$$

To solve the flow field, we follow the method developed by Ganatos *et al.* [61] and assume the stream function in the form

$$\psi = \psi_w + \psi_s, \tag{6.8}$$

where the component ψ_w is a Fourier-Bessel integral solution of Eq. (6.2) in cylindrical coordinates. This component represents the disturbance of the flow inside the microchannel in the absence of the particle, while the component ψ_s will be given in terms of spherical coordinates and represents the disturbance generated by the particle embedded in an unbounded fluid. Therefore, we have

$$\psi_w = \int_0^\infty \left(A(\tau)e^{-\tau z} + B(\tau)e^{\tau z} + C(\tau)\tau z e^{-\tau z} + D(\tau)\tau z e^{\tau z}\right)\rho J_1(\tau\rho)d\tau, \tag{6.9}$$

$$\psi_s = \sum_{n=2}^{\infty} \left(B_n r^{-n+1} + D_n r^{-n+3}\right)G_n(\zeta), \tag{6.10}$$

where G_n is the Gegenbauer polynomial of the first kind of order n and degree $-\frac{1}{2}$; A, B, C, and D are unknown functions of the separation variable τ; and B_n, D_n are unknown spherical coefficients. The general solution of the differential Eq. (6.2) can be constructed by adding the solutions given by Eqs. (6.9) and (6.10), which clearly satisfy the far-field restriction Eqs. (6.7); the cylindrical solution, ψ_w is bounded as $\rho \to 0$ and the spherical solution, ψ_s disappear as $\rho \to \infty$.

A. Solution procedure

To determine the unknown constants (B_n, D_n) and functions (A, B, C, D), we first satisfy the boundary conditions Eqs. (6.5) and (6.6) at the permeable walls of the microchannel exactly by Fourier Bessel transforms, and then the conditions at the particle surface Eqs. (6.3) and (6.4) are satisfied numerically at collocation points. Explicit expressions for the velocity components (u_ρ, u_z) are needed to satisfy the boundary conditions Eqs. (6.5) and (6.6) at the walls of the microchannel.

These expressions are obtained using Eqs. (6.1) and (6.8)–(6.10) with the aid of the spherical-cylindrical transformation [$r = \sqrt{\rho^2 + z^2}$, $\theta = \cos^{-1}(\frac{z}{\sqrt{\rho^2+z^2}})$] as follows:

$$u_\rho = \sum_{n=2}^{\infty} (B_n B_{1n} + D_n D_{1n}) + \int_0^{\infty} L(\tau, z)\tau J_1(\tau\rho)d\tau, \tag{6.11}$$

$$u_z = \sum_{n=2}^{\infty} (B_n B_{2n} + D_n D_{2n}) + \int_0^{\infty} M(\tau, z)\tau J_o(\tau\rho)d\tau, \tag{6.12}$$

where the functions ($B_{in}, D_{in},\ i = 1, 2$) and ($L(\tau, z),\ M(\tau, z)$) are defined in Appendix B. Inserting Eqs. (6.11) and (6.12) into the boundary conditions Eqs. (6.5) and (6.6) at the permeable walls of the microchannel and then inverting the resulting relations, we obtain

$$M(\tau, -z_1) = \sum_{n=2}^{\infty} (B_n b_{2n}(\tau, -z_1) + D_n d_{2n}(\tau, -z_1)), \tag{6.13}$$

$$N(\tau, -z_1) - \lambda' L(\tau, -z_1) = -\sum_{n=2}^{\infty} (B_n b_{3n}(\tau, -z_1) + D_n d_{3n}(\tau, -z_1)), \tag{6.14}$$

$$M(\tau, z_2) = \sum_{n=2}^{\infty} (B_n b_{2n}(\tau, z_2) + D_n d_{2n}(\tau, z_2)), \tag{6.15}$$

$$N(\tau, z_2) + \lambda' L(\tau, z_2) = \sum_{n=2}^{\infty} (B_n b_{3n}(\tau, z_2) + D_n d_{3n}(\tau, z_2)), \tag{6.16}$$

where

$$N(\tau, z) = \frac{d}{dz} L(\tau, z), \tag{6.17}$$

$$b_{2n}(\tau, z) = -\int_0^{\infty} B_{2n}(\rho, z)\rho J_0(\tau\rho)d\rho, \quad d_{2n}(\tau, z) = -\int_0^{\infty} D_{2n}(\rho, z)\rho J_0(\tau\rho)d\rho, \tag{6.18}$$

$$b_{3n}(\tau, z) = \int_0^{\infty} \left(B_{3n}(\tau, z) + \lambda' B_{1n}(\tau, z)\right) \rho J_1(\tau\rho)d\rho, \tag{6.19}$$

$$d_{3n}(\tau, z) = \int_0^{\infty} \left(D_{3n}(\tau, z) + \lambda' D_{1n}(\tau, z)\right) \rho J_1(\tau\rho)d\rho. \tag{6.20}$$

The integrals $b_{in},\ d_{in},\ i = 2, 3$ are calculated analytically; their values are listed in Appendix B. Substituting for $M,\ N,\ L$ given by Eqs. (B.3) and (6.17) at $z = -z_1,$ and $z = z_2$ into Eqs. (6.13)–(6.16), we obtain four algebraic equations in the unknown functions $A(\tau),\ B(\tau),\ C(\tau),\ D(\tau)$; their solutions in terms of the spherical coefficients B_n and D_n are given, respectively, by

$$A(\tau) = \sum_{n=2}^{\infty} (B_n B_{1n}^* + D_n D_{1n}^*), \quad B(\tau) = \sum_{n=2}^{\infty} (B_n B_{2n}^* + D_n D_{2n}^*), \tag{6.21}$$

$$C(\tau) = \sum_{n=2}^{\infty} (B_n B_{3n}^* + D_n D_{3n}^*), \quad D(\tau) = \sum_{n=2}^{\infty} (B_n B_{4n}^* + D_n D_{4n}^*), \tag{6.22}$$

where the functions $B_{in}^*,\ D_{in}^*,\ i = 1, 2, 3$ are defined in Appendix B. Inserting Eqs. (6.21) and (6.22) into Eqs. (B3), we obtain expressions for $L(\tau, z)$ and $M(\tau, z)$ in terms A_n and B_n, then inserting these expressions into the integral parts of the velocity components Eqs. (6.11) and (6.12), finally,

we obtain u_ρ and u_z in terms only of B_n and D_n as follows:

$$u_\rho = \sum_{n=2}^{\infty} (B_n(B_{1n} + b^*_{1n}) + D_n(D_{1n} + d^*_{1n})), \tag{6.23}$$

$$u_z = \sum_{n=2}^{\infty} (B_n(B_{2n} + b^*_{2n}) + D_n(D_{2n} + d^*_{2n})), \tag{6.24}$$

where b^*_{in}, d^*_{in}, $i = 1, 2$ are defined in Appendix B. To satisfy the boundary condition Eq. (6.4) at the surface of the particle; it is required to evaluate the tangential stress $\tau_{r\theta}$. Using the expression

$$\tau_{r\theta} = \mu\left(\frac{1}{r}\frac{\partial u_r}{\partial \theta} + r\frac{\partial}{\partial r}\left(\frac{u_\theta}{r}\right)\right), \tag{6.25}$$

the transformation relations

$$u_r = u_z \cos\theta + u_\rho \sin\theta, \quad u_\theta = -u_z \sin\theta + u_\rho \cos\theta, \tag{6.26}$$

and the expressions Eqs. (6.23) and (6.24), we obtain

$$\tau_{r\theta} = 2\mu \sum_{n=2}^{\infty} (B_n(B_{4n} + b^*_{3n}) + D_n(D_{4n} + d^*_{3n})), \tag{6.27}$$

where B_{4n}, D_{4n}, b^*_{3n}, d^*_{3n} are defined in Appendix B. The following thermal relations are also needed to satisfy the boundary condition Eq. (6.4):

$$\left.\begin{aligned} R_{3m} = \tfrac{\partial T}{r\partial\theta} &= mr^{-m-2}(P_m(\zeta)\cos\theta - P_{m-1}(\zeta))\csc\theta \\ &+ \textstyle\int_0^\infty (\sinh\varpi)^{-1}\tau^2[\cosh\sigma_2\, t_{1m}(\tau,-z_1) - \cosh\sigma_1\, t_{1m}(\tau,z_2)]\sin\theta J_0(\rho\tau)d\tau \\ &+ \textstyle\int_0^\infty (\sinh\varpi)^{-1}\tau^2[\sinh\sigma_2\, t_{1m}(\tau,-z_1) - \sinh\sigma_1\, t_{1m}(\tau,z_2)]\cos\theta(J_1(\rho\tau))d\tau. \end{aligned}\right\}, \tag{6.28}$$

$$\left.\begin{aligned} R_{4m} = \tfrac{\partial}{\partial r}\left(\tfrac{1}{r}\tfrac{\partial T}{\partial\theta}\right) = \tfrac{\partial R_{3m}}{\partial r} &= -m(m+2)r^{-m-3}(P_m(\zeta)\cos\theta - P_{m-1}(\zeta))\csc\theta \\ &+ \textstyle\int_0^\infty \tfrac{1}{2}(\sinh\varpi)^{-1}\tau^3[\sinh\sigma_2\, t_{1m}(\tau,-z_1) - \sinh\sigma_1\, t_{1m}(\tau,z_2)]\sin 2\theta J_0(\rho\tau)d\tau \\ &- \textstyle\int_0^\infty (\sinh\varpi)^{-1}\tau^3[\cosh\sigma_2\, t_{1m}(\tau,-z_1) - \cosh\sigma_1\, t_{1m}(\tau,z_2)]\sin^2\theta J_1(\rho\tau)d\tau \\ &- \textstyle\int_0^\infty (r\sinh\varpi)^{-1}\tau^2[\sinh\sigma_2\, t_{1m}(\tau,-z_1) - \sinh\sigma_1\, t_{1m}(\tau,z_2)]\cos\theta J_1(\rho\tau)d\tau. \end{aligned}\right\}. \tag{6.29}$$

Inserting Eq. (6.27)–(6.29) into the boundary conditions Eqs. (6.3) and (6.4), we obtain the following infinite set of equations for determining the unknown spherical coefficients (B_n, D_n, $n \geqslant 2$):

$$\sum_{n=2}^{\infty}(B_n((B_{1n} + b^*_{1n})\tan\theta + (B_{2n} + b^*_{2n})) + D_n((D_{1n} + d^*_{1n})\tan\theta + (D_{2n} + d^*_{2n}))) = U, \tag{6.30}$$

$$\left.\begin{aligned} &\textstyle\sum_{n=2}^{\infty}(B_n((B_{1n} + b^*_{1n})\cos\theta - (B_{2n} + b^*_{2n})\sin\theta - 2C^*_m(B_{4n} + b^*_{3n}))) \\ &\quad + \textstyle\sum_{n=2}^{\infty}(D_n((D_{1n} + d^*_{1n})\cos\theta - (D_{2n} + d^*_{2n})\sin\theta - 2C^*_m(D_{4n} + d^*_{3n}))) \\ &\quad + U\sin\theta = U^{(0)}\big(\sin\theta + \textstyle\sum_{m=0}^{\infty} R_m(R_{3m}(r,\theta) - C_{hs}R_{4m}(r,\theta))\big), \end{aligned}\right\}, \tag{6.31}$$

where $C^*_m = \frac{C_m \ell}{a}$, $C_{hs} = \frac{C_h}{C_s}$, and $U^{(0)} = \frac{\mu C_s E_\infty}{\rho_f T_0}$ is a characteristic velocity.

Again, Eqs. (6.30) and (6.31) can be satisfied using the collocation technique which is presented for the solution of the temperature field. These equations are applied at N discrete points and the infinite series in Eqs. (6.23), (6.24), and (6.27) are cut off after N terms. This produces a set of $2N$ algebraic equations for the unknown spherical coefficients B_n and D_n. The hydrodynamical variable of the fluid flow is obtained completely once the spherical coefficients are calculated for a sufficiently large number of collocation points and for various thermal and geometrical parameters of the problem.

B. Force acting on the spherical particle

The hydrodynamic drag force exerted on the spherical particle is given by [61]

$$F = 4\pi\mu D_2. \tag{6.32}$$

Since the particle is freely suspended in the fluid region, then the net force acting on the particle must vanish. Therefore, we obtain

$$D_2 = 0. \tag{6.33}$$

To determine the thermophoretic velocity U of the particle, Eq. (6.33) and the $2N$ linear algebraic equations resulting from Eqs. (6.30) and (6.31) are to be solved simultaneously. Note that the value of U is proportional to $U^{(0)}$ and dependence on the dimensionless parameters k^*, C_t^*, C_m^*, C_{hs} in addition to the length ratios among $(a,\ z_1, z_2)$.

VII. RESULTS AND DISCUSSION

The numerical results for the thermophoretic velocity of a spherical particle translating perpendicularly at an arbitrary potion between the two naturally permeable plane walls of a microchannel are presented in this section. The thermophoretic velocity is obtained using the boundary collocation method presented in the previous sections. The system of linear algebraic equations of the thermal unknown coefficients $(R_m,\ S_m)$ is constructed from Eqs. (5.8) and (5.9) while for $(B_n,\ D_n)$ is composed of Eqs. (6.30) and (6.31).

When satisfying the boundary conditions Eqs. (5.8), (5.9) and (6.30), (6.31), the first two points that will be considered along the half-circular arc of the spherical particle are $\theta = 0,\ \theta = \pi$; these two points control the gaps between the particle and the permeable plane walls of the microchannel. Also, the point $\theta = \frac{\pi}{2}$ is important because it presents the projected area of the particle normal to the direction of the particle motion. A careful inspection of the two systems of Eqs. (5.8), (5.9) and (6.30), (6.31) show that the points $\theta = 0, \frac{\pi}{2}, \pi$ are singular points of their matrix equations. To avoid this situation, these points are replaced by the following adjacent four points: $\theta = \varepsilon, \frac{\pi}{2} - \varepsilon, \frac{\pi}{2} + \varepsilon, \pi - \varepsilon$, where ε is a very small quantity. The optimum value of ε in this paper is found to be 0.01°, with which the numerical results of the thermophoretic velocity converge rapidly. More points along the generating arc are chosen as mirror-image pairs about the plane $\theta = \frac{\pi}{2}$ to divide the two quarter-circular arcs of the particle into equal segments.

A. Results of a particle in an unbounded fluid medium bounding permeable plane wall

When the upper wall of the channel is far from the particle (*i.e.*, $with z_2 \to \infty$), the particle is then migrating in an unbounded fluid medium bounding permeable plane surface. We normalize the thermophoretic velocity U with respect to the velocity for the thermophoretic motion of an identical spherical particle in an unbounded fluid, U_0, which is given by [38]

$$U_0 = 2U^{(0)}\frac{(1 + k^*C_t^*) + C_{hs}C_m^*(1 - k^* + k^*C_t^*)}{(1 + 2C_m^*)(2 + k^* + 2k^*C_t^*)}. \tag{7.1}$$

Collocation solutions of the normalized thermophoretic velocity U/U_0 are presented in Figs. 2–7 and Tables I–III for the various values of the following parameters:

(1) the spacing parameter, $0 \leqslant a/z_1 < 1$,
(2) the nondimensional permeability parameter $\lambda = a\lambda' = a\,\beta/\sqrt{K}$, $0 \leqslant \lambda < \infty$,
(3) the relative thermal conductivity $0 \leqslant k^* < \infty$,
(4) temperature jump parameter $C_t^*(= C_t\,\mathrm{Kn})$,
(5) mechanical slip parameter $C_m^*(= C_m\,\mathrm{Kn})$, and
(6) the thermal stress slip parameter $C_{hs} = C_h/C_s$.

In the literature, the following set of values has been used: $C_s = 1.17,\ C_t = 2.18,\ C_m = 1.14$, and $C_h = 1 - 3$ [36,62–64]. Therefore, the normalized coefficients C_t^* and C_m^* must be restricted

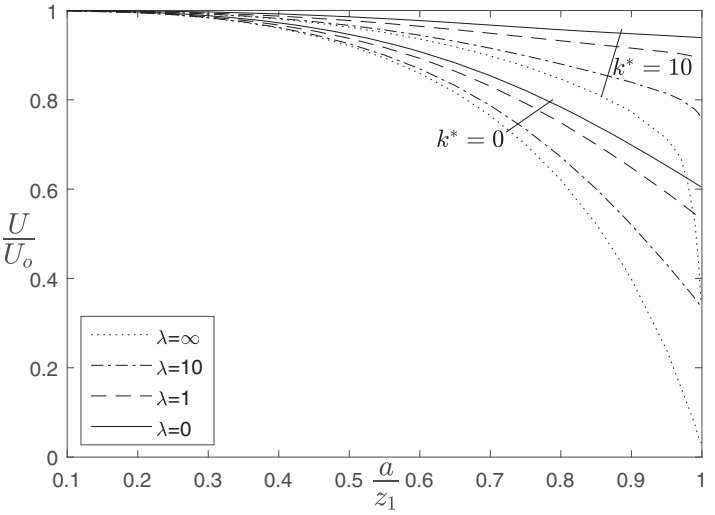

FIG. 2. Variation of the normalized thermophoretic velocity U/U_0 of a spherical particle perpendicular to a single permeable wall ($z_2 \to \infty$) against the spacing parameter a/z_1 for various values of permeability parameter λ and thermal conductivity ratio $k^* = 0,\ 10$ in the absence of thermal stress ($C_{hs} = 0$) but nonzero temperature jump and frictional slip parameters ($C_t^* = 2C_m^* = 0.02$). Note that the Knudsen number is included in the normalized coefficients C_t^* and C_m^* ($C_t^* = C_t\,\mathrm{Kn},\ C_m^* = C_m\,\mathrm{Kn}$).

to be less than unity. It is appropriate to use the ratio $C_t^*/C_m^* = 2$, since $\frac{C_t^*}{C_m^*} = \frac{C_t}{C_m} = \frac{2.18}{1.14} \approx 2$, throughout this paper. Moreover, in practice, the thermal conductivity of an aerosol particle k_p is normally greater than that of the surrounding fluid k. Therefore, the thermal conductivity ratio k^* will exceed unity under many practical applications. However, the values of $0 \leqslant k^* \leqslant 1$, which may not exist in practice, will be considered in the plotting process for the purpose of numerical comparison [42]. Note also that the value of $C_m^* = 0$ corresponds to the case of no-slip surfaces. In Eq. (7.1), $U^{(0)} = \frac{\mu E_\infty}{\rho_f T_0}$ in which $\rho_f T_0$ is a constant for an ideal gas at constant pressure. According to these equations and for aerosol particles of thermal conductivity, $k^* = 10$ and Knudsen number, $\mathrm{Kn} = 0.1$, and $E_\infty = 10^3 K/m$, Chang and Keh [38] estimated that the particles will migrate with thermophoretic velocities of order $10^{-5} m/s$. The precision and convergence behavior of the collocation/truncation technique is basically a function of the spacing parameter a/z_1. All the results calculated under this collocation scheme converge to at least five significant figures as indicated in the tables. For the case when the particle is almost in contact with the plane surface $a/z_1 = 0.99$, the number of collocation points $M = N = 50$ is sufficiently large to achieve this convergence.

1. Effect of permeability on the thermophoretic velocity

For thermal stress parameter $C_{hs} = 1$ or in the absence of thermal stress, we investigate the influences of the permeability of the wall on the normalized thermophoretic velocity through Figs. 2–4.

Figure 2 exhibits the plots of the normalized thermophoretic velocity U/U_0 versus the spacing parameter a/z_1 with thermal stress slip $C_{hs} = 0$. It indicates, for a fixed value of relative thermal conductivity, the normalized thermophoretic velocity U/U_0 is a monotonic decreasing function of a/z_1 for the entire range of the permeability parameter λ. Given a fixed value of the spacing parameter, U/U_0 decreases as the permeability parameter increases. Note that as $\lambda \to \infty$, the plane wall is completely impermeable (solid wall), while for $\lambda = 0$, the plane wall becomes a free flat surface. That is, U/U_0 has smaller values when compared with the corresponding values for the case of the free surface. Keeping the other parameter ($\lambda, C_t^*, C_m^*, a/z_1$) unchanged, the thermophoretic

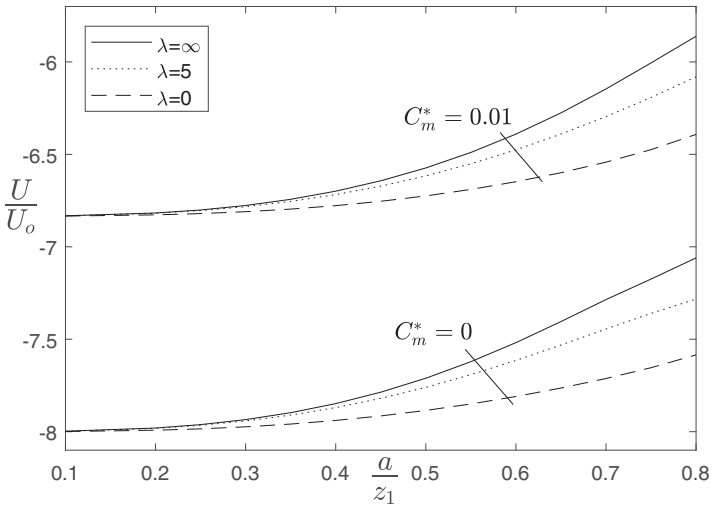

FIG. 3. Variation of the normalized thermophoretic velocity U/U_0 of a spherical particle perpendicular to a single permeable wall ($z_2 \to \infty$) against the spacing parameter a/z_1 for various values of permeability parameter λ and thermal conductivity ratio $k^* = 10$ for the case of thermal stress parameter $C_{hs} = 1$ but nonzero temperature jump and frictional slip parameters ($C_t^* = 2C_m^* = 0.02$), ($C_t^* = C_t$ Kn, $C_m^* = C_m$ Kn).

velocity increases as the relative thermal conductivity increases. Table I shows that, as expected, the particle translates with the velocity that would exist in the absence of permeable wall as $a/z_1 \to 0$, that is, $U/U_0 = 1$. Also, the collocation results in Table I for the solid plane wall ($\lambda \to \infty$) in the absence of thermal stress slip agree with the results obtained by Keh and Chang [42].

2. Effect of frictional slip and thermal stress on the thermophoretic velocity

The influences of frictional slip and thermal stress on the normalized thermophoretic velocity are investigated through Figs. 5 and 6.

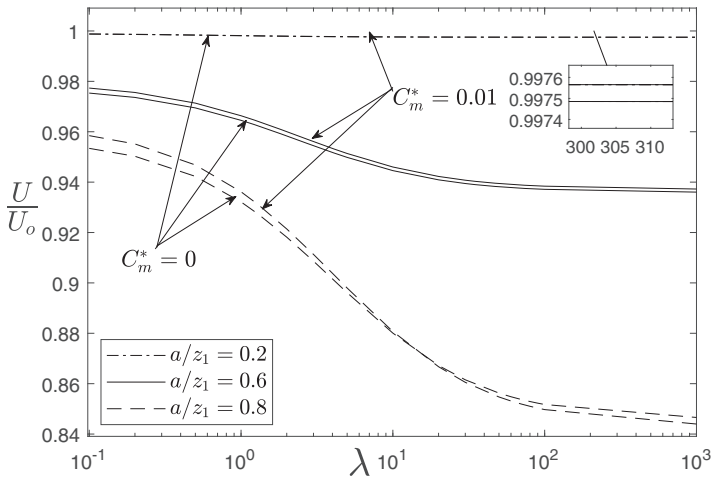

FIG. 4. Variation of the normalized thermophoretic velocity U/U_0 of a spherical particle perpendicular to a single permeable wall ($z_2 \to \infty$) against the permeability parameter λ for various values of spacing parameter a/z_1 and thermal conductivity ratio $k^* = 10$ in the absence of thermal stress ($C_{hs} = 0$) but non-zero temperature jump and frictional slip parameters ($C_t^* = 2C_m^* = 0.02$), ($C_t^* = C_t$ Kn, $C_m^* = C_m$ Kn).

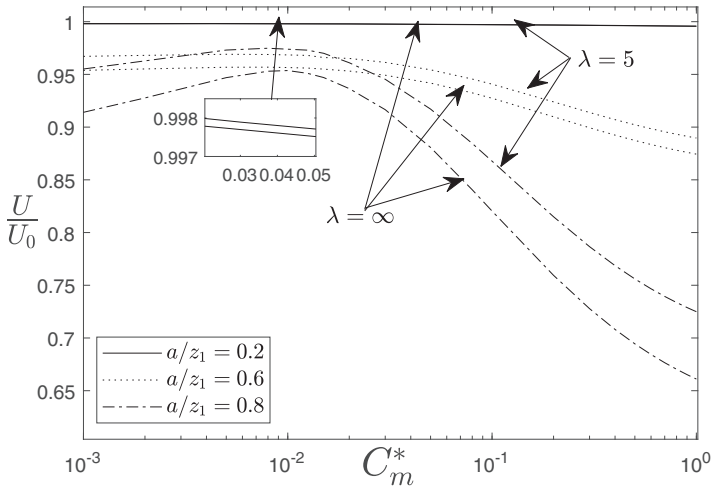

FIG. 5. Variation of the normalized thermophoretic velocity U/U_0 of a spherical particle perpendicular to a single permeable wall ($z_2 \to \infty$) against the frictional slip parameter C_m^* for various values of spacing parameter a/z_1, permeability parameter $\lambda = 5,\ \infty$ in the absence of thermal stress ($C_{hs} = 0$), and large thermal conductivity ratio $k^* = 100$ with nonzero temperature jump $C_t^* = 0.01$. Note that $\lambda \to \infty$ corresponds to a plane solid wall.

Figure 3 exhibits the plots of the normalized thermophoretic velocity U/U_0 versus the spacing parameter a/z_1 with thermal stress slip $C_{hs} = 1$. Here it should be noted that when the frictional slip C_m^* vanishes, the effect of thermal stress slip disappears, $C_{hs} = 0$. The plots for $C_m^* \neq 0$ in Fig. 3 show that the magnitude of U/U_0 decreases the function of the spacing parameter as expected. This behavior is also indicated in the collocation results of Table I. Interestingly for $C_{hs} \neq 0$ and for the values of $a/z_1 \geqslant 0.99$, the magnitude of U/U_0 increases.

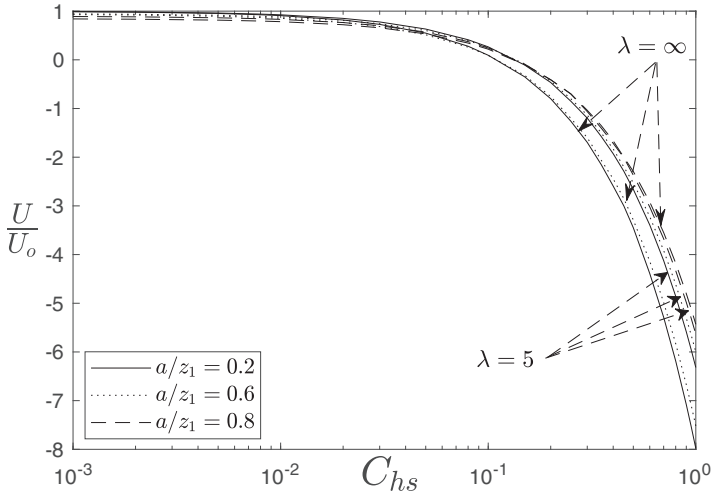

FIG. 6. Variation of the normalized thermophoretic velocity U/U_0 of a spherical particle perpendicular to a single permeable wall ($z_2 \to \infty$) against the thermal stress slip parameter C_{hs} for various values of spacing parameter a/z_1 with thermal conductivity $k^* = 10$, and nonzero temperature jump and frictional slip parameters ($C_t^* = 2C_m^* = 0.02$) for the cases of permeability parameter $\lambda = 5,\ \infty$.

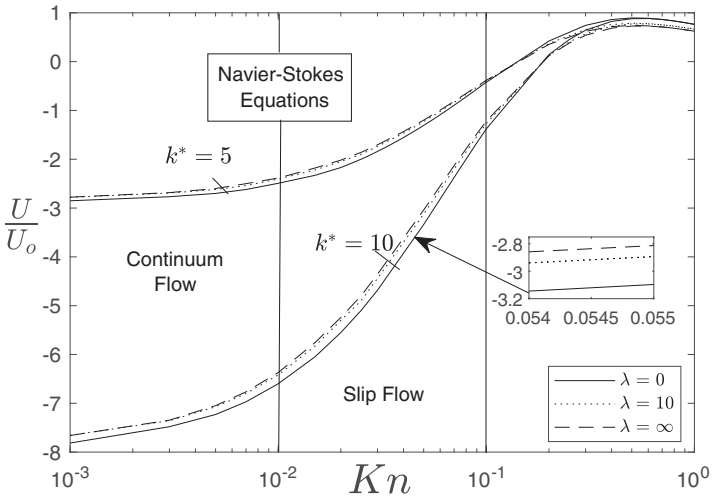

FIG. 7. Variation of the normalized thermophoretic velocity U/U_0 of a spherical particle perpendicular to a single permeable wall ($z_2 \to \infty$) against the Knudsen number (Kn) for various values of permeability parameter λ when spacing parameter $a/z_1 = 0.8$, for the case of thermal stress parameter $C_{hs} = 1$ and thermal conductivity ratio $k^* = 5, 10$. Note that the present analysis is valid for $Kn < 0.1$ while in the figure, the value of Kn is extended from 0.1 to 1 for comparison.

Figure 4 exhibits the plots of the normalized thermophoretic velocity U/U_0 versus the permeability parameter λ with $C_{hs} = 0$ for the values of $a/z_1 = 0.2,\ 0.6,\ 0.8$. Clearly, for the entire range of values of permeability parameter, $U/U_0 = 1$ as $a/z_1 \to 0$. For the values of a/z_1 near the plate, the normalized thermophoretic velocity U/U_0 decreases monotonically as the permeability parameter increases; it reaches a minimum as $\lambda \to \infty$ (solid plate). Interestingly for the values of a/z_1 very near the plate say $a/z_1 \geqslant 0.8$, the normalized thermophoretic velocity U/U_0 increases with the increase of the frictional slip C_m^* in the permeability interval $\lambda < 10$; while this behavior is reversed in $\lambda > 10$. A number of collocation results are displayed in Table II for various values of the permeability parameter.

Figure 5 exhibits the plots of the normalized thermophoretic velocity U/U_0 versus the frictional (mechanical) slip parameter C_m^* with $C_{hs} = 0$ for the values of $a/z_1 = 0.2,\ 0.6,\ 0.8$ and for the permeability cases: $\lambda = 5,\ \infty$. Note that $C_m^* = 0$ corresponds to no frictional slip at the surface of the particle. Obviously, for the entire range of C_m^* and permeability parameter, $U/U_0 \simeq 1$ as the particle far from the plate ($a/z_1 \simeq 0$). For the case of the solid plate ($\lambda \to \infty$) and when the particle is near the plate ($a/z_1 \geqslant 0.8$), the normalized thermophoretic velocity U/U_0 increases to a maximum at about $C_m^* = 0.01$ and then decreases rapidly as C_m^* increases. As the plate becomes more permeable, the thermophoretic velocity decreases slowly as C_m^* increases. A number of collocation results are displayed in Table III for some values of the frictional slip parameter.

3. Effect of Knudsen number on the thermophoretic velocity

Figure 6 exhibits the plots of the normalized thermophoretic velocity U/U_0 versus the thermal stress slip parameter C_{hs} for the values of $a/z_1 = 0.2,\ 0.6,\ 0.8$ and for the permeability cases: $\lambda = 5,\ \infty$. It should be noted here that when the thermal stress slip is included in our calculations ($C_{hs} \neq 0$), the normalized thermophoretic velocity reverses its direction. Plots indicate the magnitude of normalized thermophoretic velocity increases monotonically as C_{hs} increases. Given a fixed value of C_{hs}, the magnitude of U/U_0 increases with the permeability parameter. Again, given a fixed value of C_{hs}, the magnitude of U/U_0 decreases as the particle is getting close to the plate.

TABLE I. Collocation results of the normalized thermophoretic velocity versus the spacing parameter for various other parameters for the case of a particle migrating in an unbounded fluid medium bounding permeable plane wall.

U/U_0						
$C_{hs}=0,\ C_t^*=2C_m^*=0.02$						
	$k^*=0$			$k^*=10$		
a/z_1	$\lambda\to\infty$	$\lambda=10$	$\lambda=0$	$\lambda\to\infty$	$\lambda=10$	$\lambda=0$
0.1	0.99938	0.99938	0.99956	0.99968	0.99969	0.99987
0.3	0.9833	0.98384	0.98835	0.99165	0.99217	0.99659
0.5	0.92103	0.92538	0.94651	0.96265	0.9666	0.98584
0.7	0.76455	0.78724	0.85386	0.89844	0.91561	0.96727
0.9	0.39821	0.51994	0.69882	0.77318	0.83925	0.94778
0.95	0.24005	0.43191	0.65233	0.71327	0.81441	0.94376
0.99	0.07357	0.35564	0.61369	0.52559	0.77848	0.94012
$k^*=0, C_{hs}=1$						
	$C_t^*=2C_m^*=0$			$C_t^*=2C_m^*=0.02$		
a/z_1	$\lambda\to\infty$	$\lambda=5$	$\lambda=0$	$\lambda\to\infty$	$\lambda=5$	$\lambda=0$
0.1	–7.99751	–7.99762	–7.999	–6.83234	–6.83243	–6.83361
0.3	–7.93468	–7.94202	–7.97377	–6.7766	–6.78289	–6.81009
0.5	–7.71093	–7.76038	–7.88514	–6.57351	–6.61642	–6.72471
0.7	–7.28552	–7.44479	–7.71247	–6.14621	–6.29567	–6.54212
0.9	–7.46347	–7.16056	–7.34429	–5.66635	–5.80015	–6.12676
0.95	–8.84503	–7.02238	–7.03465	–5.65932	–5.53763	–5.85874
0.99	–14.43044	–6.49236	–6.39186	–5.01765	–5.04817	–5.45168

Figure 7 exhibits the plots of the normalized thermophoretic velocity U/U_0 versus the Knudsen number Kn when the particle near the plate ($a/z_1=0.8$) for the cases of the solid plate ($\lambda\to\infty$), $\lambda=10$ and free surface ($\lambda=0$) at thermal conductivities ratios $k^*=5,10$. Plots indicate that in the slip flow region ($0.01<\mathrm{Kn}<0.1$), the magnitude of normalized thermophoretic velocity U/U_0 decreases as Kn increases. Given a fixed value of Kn in the slip flow region, the

TABLE II. Collocation results of the normalized thermophoretic velocity versus the permeability parameter for different values of the spacing parameter with $k^*=10$ and $C_t^*=2C_m^*=0,\ 0.02$ for the case of a particle migrating in an unbounded fluid medium bounding permeable plane wall.

U/U_0						
	$k^*=10, C_t^*=2C_m^*=0$			$k^*=10, C_t^*=2C_m^*=0.02$		
λ	$a/z_1=0.2$	$a/z_1=0.6$	$a/z_1=0.8$	$a/z_1=0.2$	$a/z_1=0.6$	$a/z_1=0.8$
0	0.99903	0.97933	0.96208	0.998953	0.977316	0.95689
10	0.99766	0.946	0.88072	0.997584	0.944567	0.880069
30	0.9976	0.94076	0.86053	0.997514	0.93945	0.861536
50	0.99758	0.93945	0.85472	0.997499	0.938174	0.856259
70	0.99757	0.93886	0.85194	0.997493	0.937593	0.853742
90	0.99757	0.93852	0.8503	0.997489	0.937261	0.852265
100	0.99756	0.93726	0.84398	0.997488	0.937143	0.851735

TABLE III. Collocation results of the normalized thermophoretic velocity versus the frictional slip parameter for different values of the spacing parameter with $k^* = 100$, $C_t^* = 2C_m^*$ for the case of a particle migrating in an unbounded fluid medium bounding.

	U/U_0					
	$k^* = 100, \lambda = 5$			$k^* = 100, \lambda \to \infty$		
C_m^*	$a/z_1 = 0.2$	$a/z_1 = 0.6$	$a/z_1 = 0.8$	$a/z_1 = 0.2$	$a/z_1 = 0.6$	$a/z_1 = 0.8$
0	0.998199	0.965557	0.943099	0.998	0.95175	0.89311
0.1	0.997361	0.940733	0.867695	0.99716	0.92738	0.82039
0.3	0.996581	0.913867	0.786629	0.99638	0.8994	0.72783
0.5	0.996215	0.902203	0.756007	0.99601	0.88735	0.69443
0.7	0.996001	0.895577	0.739415	0.9958	0.8805	0.67655
0.9	0.995861	0.891281	0.728898	0.99566	0.87606	0.66528
1	0.995808	0.88965	0.72495	0.99563	0.87438	0.66105

magnitude of normalized thermophoretic velocity U/U_0 is greater for the free surface than that of a solid plate. Again, given a fixed value of Kn, the magnitude of U/U_0 increases as with the increase of thermal conductivity ratio k^*. It should be noted here that, as we mentioned earlier, our model is also valid in the continuum flow Kn < 0.01. Therefore, the Navier-Stokes equation is valid in the continuum-slip region in which Kn < 0.1.

In other words, our results are obtained on the basis of a continuum model for the gas phase with a slip flow boundary condition at the interface between particle and gas. It is worth mentioning the following example: for a perfect gas, the mean-free path of gas molecules is inversely proportional to the pressure. The mean-free path of air molecules at 25 °C is about 67 nm at 1 atm and about 51 μm at 1 torr [65]. Therefore, the present results are applicable for a wide range (about 0.5 m or larger) of particle sizes around atmospheric pressure. Moreover, it is applicable also for relatively large particles (about 0.1 mm or larger) at low pressures [42]. Once again, in our continuum-with-slippage approach given above, the Knudsen number of the system should be smaller than 0.1 in this case; the mean-free path in the fluid is not on the order of the size of the particle, which justifies the assumption of a thin Knudsen layer at the surface of the particle mentioned earlier. However, in some flows, the Knudsen number is relatively large, the Navier-Stokes equations based on the continuum assumption will fail to work for such flows, and the Knudsen layer is no longer thin. Therefore, other governing equations are needed to treat these flows. Figure 8 shows the streamlines for the flow around a spherical particle in an unbounded fluid medium in the presence of a permeable plane wall. The streamlines are clearly deflected due to the presence of the permeable wall.

B. Results of spherical particle inside permeable microchannel

Here we present the collocation solutions of the normalized thermophoretic velocity of the spherical particle U/U_0 moving perpendicularly to the permeable walls of a microchannel. Collocation solutions of U/U_0 are presented in Figs. 9–12 and Tables IV–VI for the various values of the parameters considered in subsection A in addition to the parameter a/z_2, where z_2 represents the distance between the particle center and the upper wall of the microchannel. Throughout our calculations, we consider $a/z_2 = a/z_1$; that is, the center of the particle at the instant it passes the centerline of the microchannel.

1. Effect of permeability on the thermophoretic velocity

Here, we investigate the influences of the permeability of the walls of the microchannel on the normalized thermophoretic velocity through Figs. 9–11.

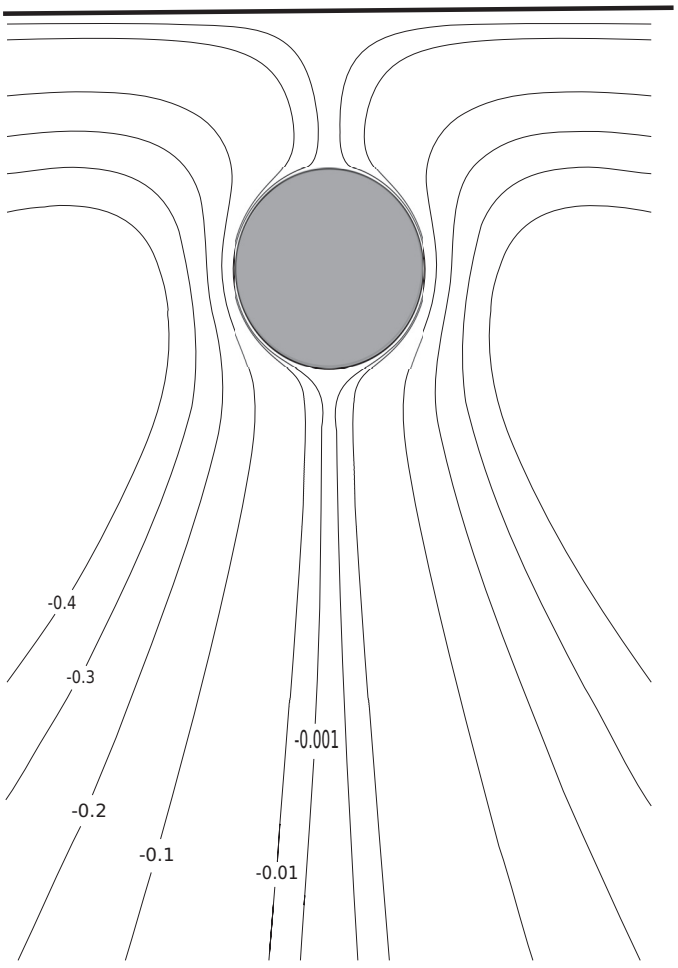

FIG. 8. Streamlines for the flow around spherical particle in an unbounded fluid medium in the presence of a plane wall with $z_1/a = 3$, $k^* = 10$, $C_t^* = 2C_m^* = 0.02$, $C_{hs} = 1$, and $\lambda \to \infty$.

Figure 9 exhibits the plots of the normalized thermophoretic velocity U/U_0 for a particle in a microchannel versus the spacing parameter $a/z_1 (= a/z_2)$ for the case without thermal stress $C_{hs} = 0$ but nonzero temperature jump parameter k^* in the absence of thermal stress (C_{hs}) but nonzero temperature jump and frictional slip parameters $C_t^* \neq 0$. The plots show that for $k^* = 0$, that is, when the particle is thermally insulated, the normalized thermophoretic velocity U/U_0 decreases monotonically as a/z_1 increases for the entire range of permeability parameter λ with lowest values of U/U_0 near the walls of the channel. It also shows that for a fixed value of the spacing parameter $a/z_1 (= a/z_2)$, U/U_0 decreases as the permeability parameter increases with maximum and minimum values of U/U_0 occuring, respectively, for the channel of solid walls $\lambda \to \infty$ and for the channel with free surfaces ($\lambda = 0$).The above behavior is different for the case of a large ratio in the thermal conductivity of particle and fluid ($k^* = 10$). We find that for $\lambda > \lambda_c$ with $\lambda_c = 4$, there is a steep increase in the normalized thermophoretic velocity U/U_0 when the particle is close to the walls of the channel. For $\lambda < \lambda_c$, there is a slight decrease in U/U_0 as a/z_1 increases and for the case of solid walls, U/U_0 decreases sharply as the particle approaches the walls of the channel. Clearly, the behavior of the normalized velocity of the particle changes considerably with the permeability of the channel walls in the case of the large values of the thermal conductivity ratio. That means the

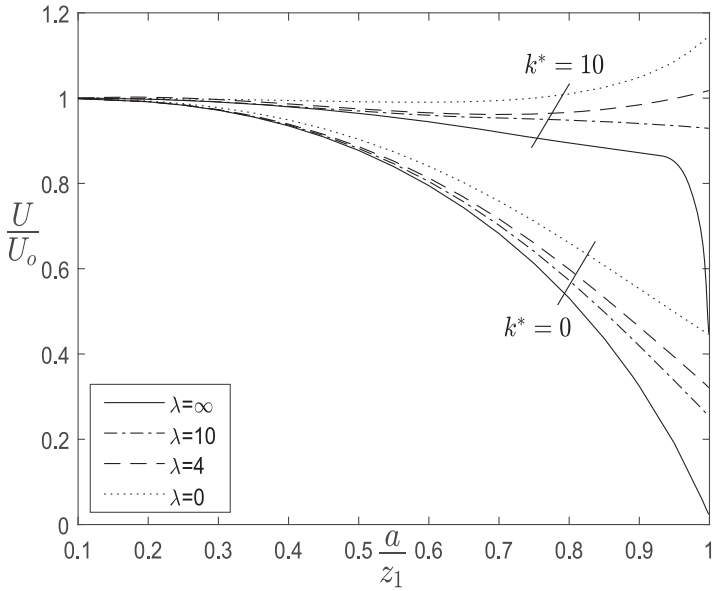

FIG. 9. Variation of the normalized thermophoretic velocity U/U_0 of a spherical particle moving perpendicularly to the permeable walls of a microchannel against the spacing parameter $a/z_1 (= a/z_2)$ for various values of permeability parameter λ and thermal conductivity $k^* = 0,\ 10$ in the absence of thermal stress ($C_{hs} = 0$) but nonzero temperature jump and frictional slip parameters ($C_t^* = 2C_m^* = 0.02$).

permeability of the walls can affect the fluid flow near the walls. When the walls are impermeable (rigid), the fluid flow is confined to a thin layer near each wall, creating a strong thermal gradient and large thermophoretic force which makes the thermophoretic velocity of the particle decrease sharply near the walls (the solid plot in Fig. 9). However, when the channel walls are permeable, the fluid creates a different flow pattern and different temperature gradient near the walls ($a/z_1 > 0.8$). It can penetrate the wall, which can lead to a speedup of the thermophoretic velocity of the particle. This behavior is in contrast, under the same set of parameters, to the case of only one permeable plate, see Fig. 2.

Figure 10 exhibits the plots of the normalized thermophoretic velocity U/U_0 versus the relative thermal conductivity k^* with thermal stress slip $C_{hs} = 0,\ 1$. Plots of Fig. 10(a) for $C_{hs} = 0$ show

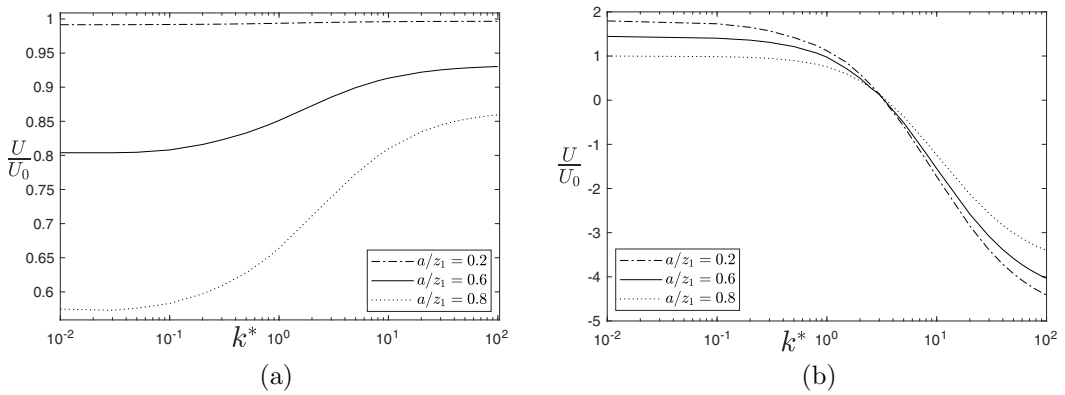

FIG. 10. Variation of the normalized thermophoretic velocity U/U_0 against the relative thermal conductivity k^* for different values of $a/z_1 = a/z_2$ and $\lambda = 10,\ C_t^* = 2C_m^* = 0.02$; (a) $C_{hs} = 0$, (b) $C_{hs} = 1$.

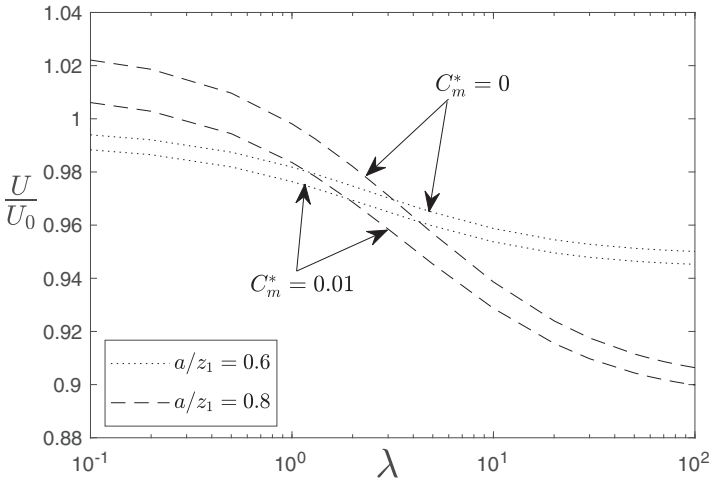

FIG. 11. Variation of the normalized thermophoretic velocity U/U_0 against the permeability parameter λ with $C_{hs} = 0,\ k^* = 10,\ C_t^* = 2C_m^* = 0,\ 0.02$.

that the normalized thermophoretic velocity U/U_0 is a monotonic increasing function of k^* when the particle is near the permeable walls of the microchannel ($a/z_1 > 0.6$); while when the particle is far from the walls, U/U_0 is almost constant function in k^*. For a given value of k^*, the normalized thermophoretic velocity U/U_0 increases as a/z_1 decreases. For values of C_{hs} different from zero, Fig. 10(b) shows a significant variation of U/U_0 when compared with the case of $C_{hs} = 0$. It indicates that for the entire range of spacing parameter a/z_1, the normalized thermophoretic velocity U/U_0 decreases as k^* increases—it vanishes at about $k^* = 2$. For $k^* > 2$, the particle reverses its direction of motion and the magnitude of U/U_0 increases.

2. Effect of thermal conductivity on the thermophoretic velocity

For thermal stress parameter $C_{hs} = 1$ or in the absence of thermal stress, we investigate the influences of thermal conductivity on the normalized thermophoretic velocity through Fig. 11.

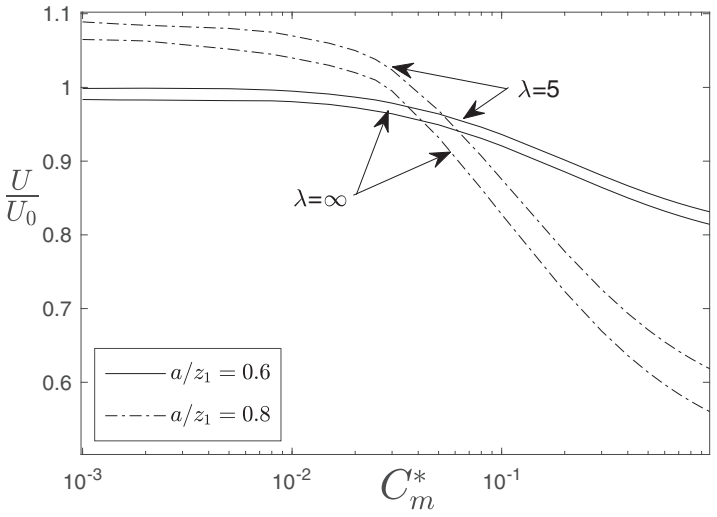

FIG. 12. Variation of the normalized thermophoretic velocity U/U_0 against the frictional slip parameter C_m^* for values of $a/z_1 = 0.6,\ 0.8$ with $\lambda = 5, \infty,\ k^* = 100,\ C_t^* = 2C_m^*$.

TABLE IV. Collocation results of the normalized thermophoretic velocity versus $a/z_1 = a/z_2$ for different values of the permeability parameter with $k^* = 0,\ 10,\ C_{hs} = 0$ and $C_t^* = 2C_m^* = 0.02$.

U/U_0						
$C_t^* = 2C_m^* = 0.02 \quad C_{hs} = 0$						
	$k^* = 0$			$k^* = 10$		
a/z_1	$\lambda \to \infty$	$\lambda = 10$	$\lambda = 0$	$\lambda \to \infty$	$\lambda = 10$	$\lambda = 0$
0.1	0.99892	0.99893	0.99916	0.99964	0.99965	0.99988
0.3	0.97173	0.97242	0.97786	0.99107	0.99177	0.99729
0.5	0.87727	0.88197	0.90361	0.96444	0.96923	0.99164
0.7	0.68228	0.70204	0.7586	0.91997	0.95371	0.99432
0.9	0.32454	0.41908	0.55289	0.87203	0.9365	1.04906
0.95	0.19034	0.33723	0.49817	0.85236	0.93443	1.08593
0.99	0.05596	0.27018	0.4552	0.66675	0.93226	1.13178
$C_t^* = 2C_m^* = 0.02 \quad C_{hs} = 1$						
	$k^* = 0$			$k^* = 10$		
a/z_1	$\lambda \to \infty$	$\lambda = 5$	$\lambda = 0$	$\lambda \to \infty$	$\lambda = 5$	$\lambda = 0$
0.1	1.97853	1.97809	1.97805	–6.83371	–6.83219	–6.83205
0.3	1.93636	1.92665	1.92421	–6.81621	–6.78235	–6.77386
0.5	1.78934	1.75263	1.73718	–6.78561	–6.66142	–6.61053
0.7	1.50218	1.41152	1.35105	–6.88467	–6.66346	–6.54276
0.9	1.09484	0.89628	0.64266	–7.51812	–7.6932	–8.45965
0.95	0.98647	0.75181	0.37691	–7.69469	–8.2668	–10.67758
0.99	0.90138	0.6334	0.11262	–7.54179	–8.47453	–12.56126

Figure 11 exhibits the plots of the normalized thermophoretic velocity U/U_0 versus the permeability parameter λ with spacing parameter $a/z_1 = 0.6,\ 0.8$ and $C_{hs} = 0,\ k^* = 10,\ C_t^* = 2C_m^* = 0,\ 0.02$. As expected, the normalized thermophoretic velocity is a monotonically decreasing function of permeability parameter λ. Clearly, the normalized thermophoretic velocity slows down faster for frictional slip cases, $C_m^* \neq 0$, than that in the case of no-slip, $C_m^* = 0$.

TABLE V. Collocation results of the normalized thermophoretic velocity versus the permeability parameter for different values of the spacing parameter with $k^* = 10$ and $C_{hs} = 0,\ C_t^* = 2C_m^* = 0,\ 0.02$.

U/U_0						
	$k^* = 10,\ C_t^* = 2C_m^* = 0$			$k^* = 10,\ C_t^* = 2C_m^* = 0.02$		
λ	$a/z_1 = 0.2$	$a/z_1 = 0.6$	$a/z_1 = 0.8$	$a/z_1 = 0.2$	$a/z_1 = 0.6$	$a/z_1 = 0.8$
0	0.9993	0.99608	1.0259	0.99911	0.99042	1.00969
10	0.99755	0.95874	0.93861	0.99736	0.95371	0.92869
30	0.99746	0.95278	0.91755	0.99726	0.94789	0.90973
50	0.99744	0.95129	0.91154	0.99724	0.94643	0.90439
70	0.99743	0.95062	0.90867	0.99723	0.94577	0.90185
90	0.99742	0.95023	0.90698	0.99723	0.9454	0.90036
100	0.99742	0.95009	0.90638	0.99722	0.94526	0.89983

TABLE VI. Collocation results of the normalized thermophoretic velocity versus the frictional slip parameter for different values of the spacing parameter with $C_{hs} = 0,\ k^* = 100,\ \lambda = 5,\ \infty$.

	U/U_0					
	$k^* = 100,\ \lambda = 5$			$k^* = 100,\ \lambda \to \infty$		
C_m^*	$a/z_1 = 0.2$	$a/z_1 = 0.6$	$a/z_1 = 0.8$	$a/z_1 = 0.2$	$a/z_1 = 0.6$	$a/z_1 = 0.8$
0	0.99874	0.99769	1.06456	0.99847	0.98147	1.00817
0.1	0.99673	0.93618	0.87544	0.99645	0.92074	0.82792
0.3	0.99488	0.88067	0.7259	0.9946	0.86437	0.66955
0.5	0.99401	0.85653	0.67116	0.99373	0.83992	0.61356
0.7	0.9935	0.84289	0.64217	0.99322	0.82609	0.58419
0.9	0.99317	0.83409	0.6241	0.99289	0.81716	0.56595
1	0.99304	0.83076	0.61738	0.99276	0.81378	0.55919

3. Effect of frictional slip on the thermophoretic velocity

Here, we investigate the influences of frictional slip on the normalized thermophoretic velocity through Fig. 12.

Figure 12 exhibits the plots of the normalized thermophoretic velocity U/U_0 versus the frictional slip parameter C_m^* with spacing parameter $a/z_1 = 0.6,\ 0.8$ and permeability parameter $\lambda = 5, \infty$.

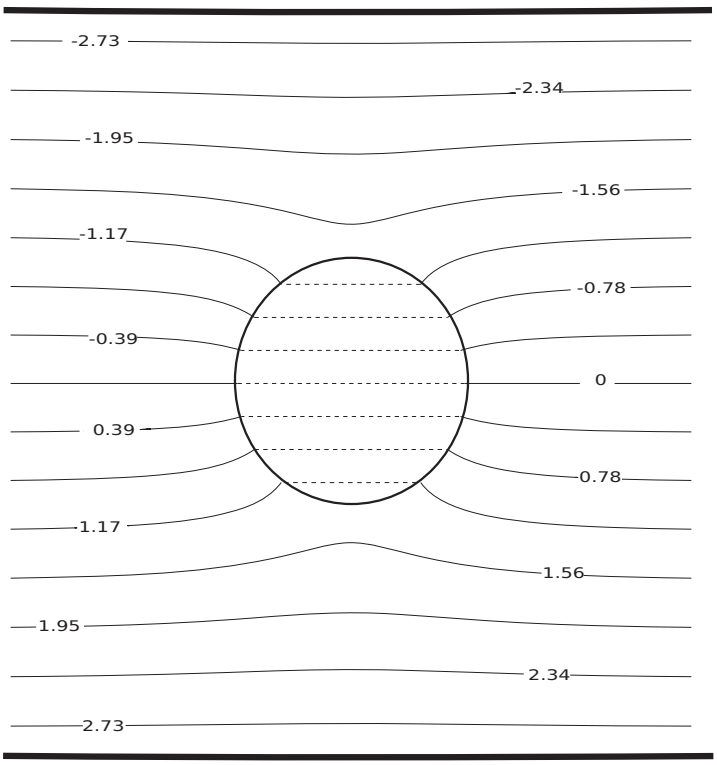

FIG. 13. Temperature contours (isothermal curves) of a spherical particle situated at the centerline of a microchannel ($z_1/a = z_2/a = 3$) with $k^* = 0$. (Note that when the thermal conductivity ratio vanishes, the temperature distributions are independent of Knudsen number).

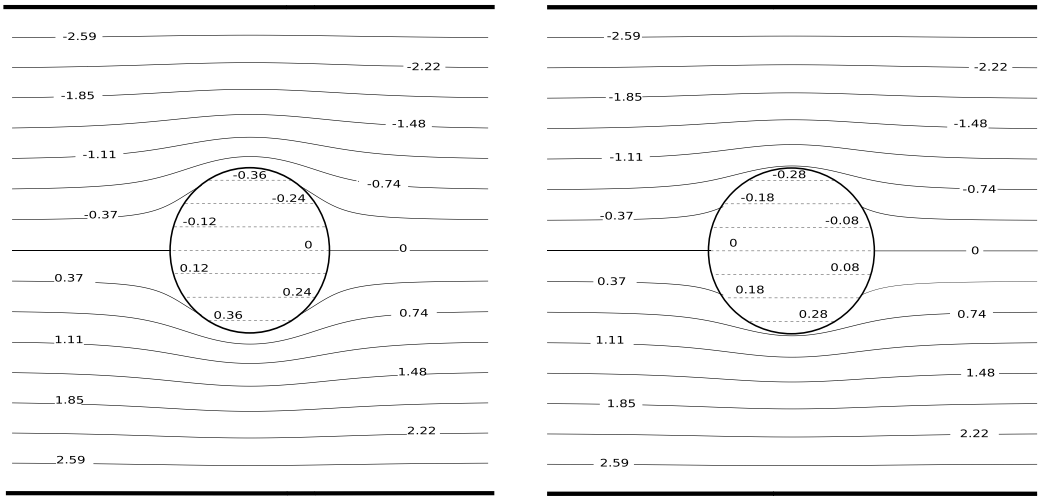

(a) (b)

FIG. 14. Temperature contours (isothermal curves) of a spherical particle situated at the centerline ($z_1/a = z_2/a = 3$) of a microchannel with (a) $k^* = 5$, $\mathrm{Kn} = 0.01$, (b) $k^* = 5$, $\mathrm{Kn} = 0.1$.

Again, the normalized thermophoretic velocity is a monotonically decreasing function of the frictional slip parameter C_m^*. Clearly, the case of no slip surface $C_m^* = 0$ has maximum values of U/U_0 when compared with the case of perfect slip $C_m^* \to \infty$, a gas bubble particle. A number of convergent collocation results are displayed in Tables V and VI for various values of the permeability and frictional slip parameters.

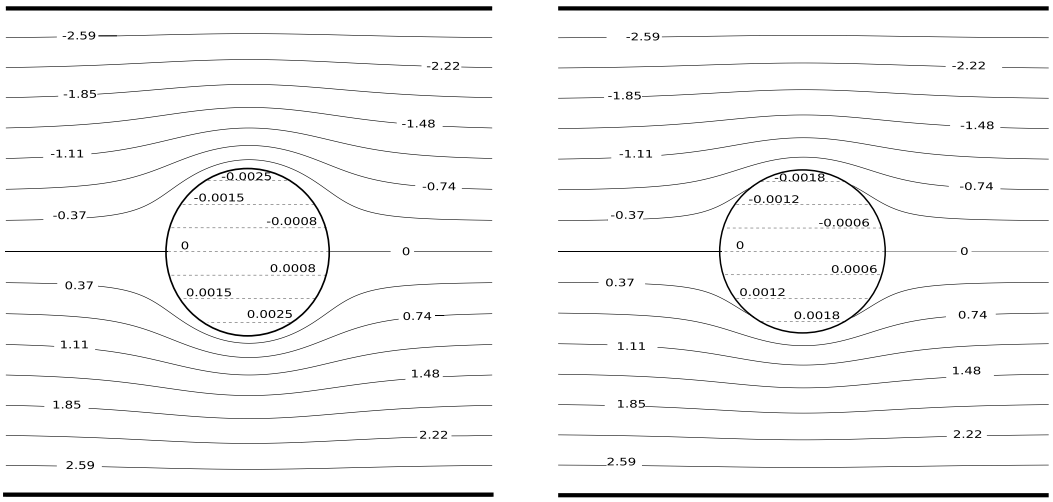

(a) (b)

FIG. 15. Temperature contours (isothermal curves) of a spherical particle situated at the centerline ($z_1/a = z_2/a = 3$) of a microchannel with (a) $k^* \to \infty$, $\mathrm{Kn} = 0.01$, (b) $k^* \to \infty$, $\mathrm{Kn} = 0.1$.

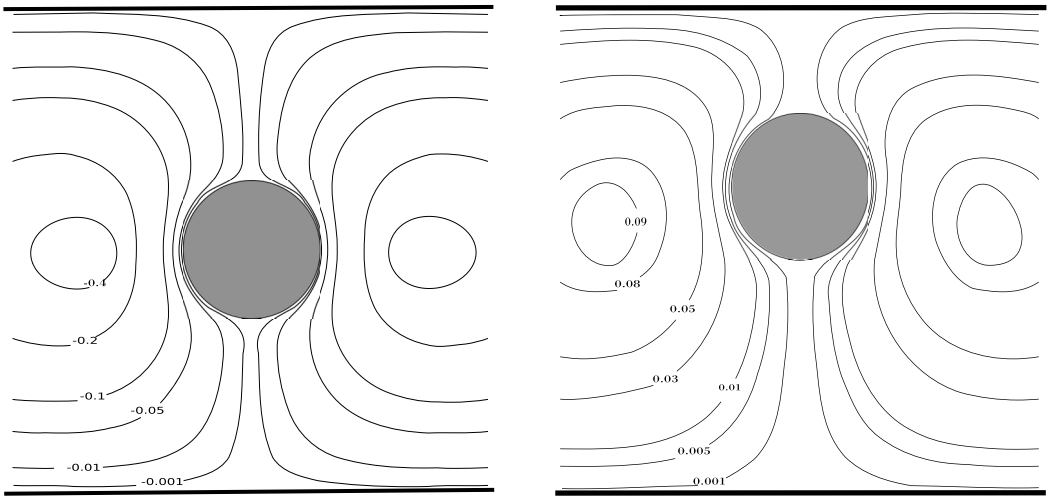

(a) (b)

FIG. 16. Streamlines for the flow around spherical particle immersed in a microchannel with $k^* = 100$, $C_t^* = 2C_m^* = 0.2$, $C_{hs} = 0$ and $\lambda \to \infty$ situated at $(z_1/a = z_2/a = 4)$ and $z_1/a = 5$, $z_2/a = 3$.

4. Temperature contours

Here, the contour plots of fluid and particle temperatures are shown in Figs. 13–15 for the case when the spherical particle is situated at the centerline of a microchannel $(z_1/a = z_2/a = 3)$ with a combination of the parameters: Knudsen number $\mathrm{Kn} = 0.1,\ 0.01$ and particle to fluid thermal conductivity ratio $k^* = 0,\ 5,\ \infty$.

Figure 13 exhibits a sketch of the isotherms inside and around a spherical particle situated at the centerline of a microchannel $(z_1/a = z_2/a = 3)$ with $k^* = 0$. Plots indicate that no temperature jump at the surface of the particle and the temperatures are independent of the Knudsen number. This behavior is clear from the boundary conditions Eqs. (5.1) and (5.2) by setting $k^* = 0$ $(k^* = k_p/k)$. Figure 14 exhibits a sketch of the isotherms of the system with nonzero value of the thermal conductivity ratio $(k^* = 5)$ for two different values of Knudsen number (a) $\mathrm{Kn} = 0.01$, (b) $\mathrm{Kn} = 0.1$. Figure 15 is the same as Fig. 14 but with $k^* \to \infty$. Figures show no temperature deviation inside the spherical particle and temperature jumps across the spherical surface are clear.

We have also sketched some of the streamlines in Fig. 16 to achieve a more complete understanding of the thermophoretic migration of a spherical particle inside a permeable microchannel at different locations from the permeable walls of the microchannel. The streamlines are clearly deflected due to the presence of the permeable walls [66].

VIII. CONCLUSION

In this paperm the quasisteady axisymmetric thermophoretic slow motion of a spherical particle situated at an arbitrary position inside a microchannel with parallel permeable plane walls is studied theoretically in the limit of negligible Péclet number. A particular case is also treated, that is, the axisymmetric thermophoretic slow motion of a slip particle towards a permeable plane wall. A uniform temperature gradient is imposed perpendicular to the permeable walls of the microchannel. The Knudsen number Kn is assumed to be in the range $0.01 < \mathrm{Kn} < 0.1$ so the fluid flow is modeled by a continuum approach with a temperature jump, a creeping slip, a frictional slip, and a thermal stress slip at the surface of the particle. A semianalytical approach with the boundary collocation method has been used to solve the Stokes equations for the fluid flow field. In this paper, we considered two effects: the effect of permeability of the walls of the microchannel and the effect

of thermal stress slip on the thermophoretic velocity of the particle. The purpose of this paper is to evaluate the thermophoretic velocity of a spherical particle moving axisymmetrically inside a permeable microchannel. The results of the thermophoretic velocity of the particle show that the solution procedure converges rapidly with excellent accuracy for various values of the thermal, mechanical, and geometric parameters of the problem. Calculations of the thermophoretic velocity include the special case of the microchannel with solid walls. The major findings of the present paper may be outlined as follows:

(1) Increasing the permeability parameter λ of the microchannel walls causes a slowing down of the thermophoretic velocity of the particle. The particle tends to its lowest thermophoretic velocity as $\lambda \to \infty$ (impermeable walls) and reaches its maximum velocity as $\lambda = 0$ (free surfaces).

(2) It found that the thermal stress slip parameter has significant effects on the normalized thermophoretic velocity.

(3) The thermophoretic velocity slows down sharply as the particle becomes near contact with the sides of the microchannel.

(4) For the entire permeability parameter, the thermophoretic velocity slows down as the frictional slip parameter increases. Values of the thermophoretic velocity are maximum for the case of a no-frictional slip, $C_m^* = 0$.

(5) For the case when neglecting the effect of the thermal stress slip, the thermophoretic velocity speeds up as the relative conductivity ratio increases when the particle is near the walls of the microchannel with an irrelevant effect when the particle is far from the walls.

This paper is inspired by its wide variety of flows where solid particles interact with a naturally permeable boundary. In particular, it's important in the study of near-wall microfluidics in the proximity of the glycocalyx surface layer on vascular endothelium and in microelectromechanical systems devices where charged macromolecules may become adsorbed to microchannel walls [49].

APPENDIX A

$$R_{1m} = r^{-m-1}P_m(\zeta) + \int_0^\infty (\sinh\,\varpi)^{-1}[\,t_{1m}(\tau, z_2)\sinh\sigma_1 - t_{1m}(\tau, -z_1)\sinh\sigma_2]\tau J_0(\rho\tau)d\tau, \quad \text{(A1)}$$

$$S_{1m} = r^m P_m(\zeta), \quad \varpi = \tau(z_1 + z_2), \quad \sigma_1 = \tau(z + z_1), \quad \sigma_2 = \tau(z - z_2), \quad \text{(A2)}$$

$$t_{1m}(\tau, z) = -\frac{\tau^{m-1}}{m!}\left(\frac{|z|}{z}\right)^m e^{-|z|\tau}. \quad \text{(A3)}$$

Here $J_n(\rho\tau)$ is the Bessel function of first kind and order n, and $P_n(\zeta)$ is the Legendre polynomial of order n.

$$\begin{aligned} R_{2m} &= \frac{\partial R_{1m}}{\partial r} \\ &= -(m+1)r^{-m-2}P_m(\zeta) \\ &\quad + \int_0^\infty \tau^2(\sinh\,\varpi)^{-1}\begin{bmatrix}(\,t_{1m}(\tau, z_2)\cosh\sigma_1 - t_{1m}(\tau, -z_1)\cosh\sigma_2\,)\cos\theta J_0(\rho\tau)\\ -(\,t_{1m}(\tau, z_2)\sinh\sigma_1 - t_{1m}(\tau, -z_1)\sinh\sigma_2)\sin\theta J_1(\rho\tau)\end{bmatrix}d\tau. \end{aligned} \quad \text{(A4)}$$

APPENDIX B

$$\left.\begin{aligned} B_{1n} &= -(n+1)r^{-n-1}G_{n+1}(\zeta)\csc\theta \\ D_{1n} &= -r^{-n+1}((n+1)G_{n+1}(\zeta)\csc\theta - 2G_n(\zeta)\cot\theta)\end{aligned}\right\}, \quad \text{(B1)}$$

$$\left.\begin{aligned} B_{2n} &= -r^{-n-1}P_n(\zeta) \\ D_{2n} &= -r^{-n+1}(2G_n(\zeta)+P_n(\zeta)) \end{aligned}\right\}, \tag{B2}$$

$$\left.\begin{aligned} L(\tau,z) &= (-A(\tau)e^{-\tau z}+B(\tau)e^{\tau z}+C(\tau)(1-\tau z)e^{-\tau z}+D(\tau)(1+z\tau)e^{\tau z}) \\ M(\tau,z) &= -(A(\tau)e^{-\tau z}+B(\tau)e^{\tau z}+C(\tau)\tau z e^{-\tau z}+D(\tau)\tau z e^{\tau z}) \end{aligned}\right\}, \tag{B3}$$

$$\left.\begin{aligned} b_{2n} &= \tfrac{\tau^{n-1}}{n!}\left(\tfrac{|z|}{z}\right)^n e^{-|z|\tau} \\ d_{2n} &= \tfrac{\tau^{n-3}}{n!}\left(\tfrac{|z|}{z}\right)^n e^{-|z|\tau}((2n-3)\tau|z|-(n-1)(n-3)) \end{aligned}\right\}, \tag{B4}$$

$$\left.\begin{aligned} b_{3n} &= \tfrac{-\tau^{n-1}}{n!}\left(\tfrac{|z|}{z}\right)^n e^{-|z|\tau}\left(\lambda'\tfrac{z}{|z|}-\tau\right) \\ d_{3n} &= \tfrac{1}{n!}\left(\tfrac{|z|}{z}\tau\right)^{n-3} e^{-|z|\tau}\left((2n-3)\tau|z|\left(\tau\tfrac{|z|}{z}-\lambda'\right)+\left(n(n-2)\lambda'-(n^2-3)\tfrac{|z|}{z}\tau\right)\right) \end{aligned}\right\}, \tag{B5}$$

$$\left.\begin{aligned} B^*_{1n} &= \tfrac{1}{\Delta}(\delta_1 b_{2n}(\tau,-z_1)+\delta_2 b_{2n}(\tau,z_2)+\delta_3 b_{3n}(\tau,-z_1)+\delta_4 b_{3n}(\tau,z_2)) \\ D^*_{1n} &= \tfrac{1}{\Delta}(\delta_1 d_{2n}(\tau,-z_1)+\delta_2 d_{2n}(\tau,z_2)+\delta_3 d_{3n}(\tau,-z_1)+\delta_4 d_{3n}(\tau,z_2)) \end{aligned}\right\}, \tag{B6}$$

$$\left.\begin{aligned} B^*_{2n} &= \tfrac{1}{\Delta}(\delta_5 b_{2n}(\tau,-z_1)+\delta_6 b_{2n}(\tau,z_2)+\delta_7 b_{3n}(\tau,-z_1)+\delta_8 b_{3n}(\tau,z_2)) \\ D^*_{2n} &= \tfrac{1}{\Delta}(\delta_5 d_{2n}(\tau,-z_1)+\delta_6 d_{2n}(\tau,z_2)+\delta_7 d_{3n}(\tau,-z_1)+\delta_8 d_{3n}(\tau,z_2)) \end{aligned}\right\}, \tag{B7}$$

$$\left.\begin{aligned} B^*_{3n} &= \tfrac{1}{\Delta}(\delta_9 b_{2n}(\tau,-z_1)+\delta_{10} b_{2n}(\tau,z_2)+\delta_{11} b_{3n}(\tau,-z_1)+\delta_{12} b_{3n}(\tau,z_2)) \\ D^*_{3n} &= \tfrac{1}{\Delta}(\delta_9 d_{2n}(\tau,-z_1)+\delta_{10} d_{2n}(\tau,z_2)+\delta_{11} d_{3n}(\tau,-z_1)+\delta_{12} d_{3n}(\tau,z_2)) \end{aligned}\right\}, \tag{B8}$$

$$\left.\begin{aligned} B^*_{4n} &= \tfrac{1}{\Delta}(\delta_{13} b_{2n}(\tau,-z_1)+\delta_{14} b_{2n}(\tau,z_2)+\delta_{15} b_{3n}(\tau,-z_1)6+\delta_{16} b_{3n}(\tau,z_2)) \\ D^*_{4n} &= \tfrac{1}{\Delta}(\delta_{13} d_{2n}(\tau,-z_1)+\delta_{14} d_{2n}(\tau,z_2)+\delta_{15} d_{3n}(\tau,-z_1)+\delta_{16} d_{3n}(\tau,z_2)) \end{aligned}\right\}, \tag{B9}$$

$$\Delta = 2e^{-2\varpi}(\lambda'-2\tau)^2+e^{2\varpi}(\lambda'+2\tau)^2-2(4\tau^2+\lambda'(\lambda'+4\varpi(2\tau+\lambda'\varpi^2))). \tag{B10}$$

$$\left.\begin{aligned} \delta_1 &= e^{z_2\tau+\varpi}(\lambda'+2\tau)(\tau(-2-z_1\tau)+\lambda'(-1-z_1\tau))+e^{z_2\tau-\varpi}(-2\tau^2(-2+z_2\tau+\varpi) \\ &\quad +\lambda'\tau(-4+3\varpi+z_2\tau(5-2\varpi))+\lambda'^2(1-\varpi+z_2\tau(-1+2\varpi))) \\ \delta_2 &= e^{-z_1\tau-\varpi}(-\lambda'+2\tau)(\tau(-2+z_2\tau)+\lambda'(1-z_2\tau))+e^{-z_1\tau+\varpi}(2\tau^2(2+z_1\tau+\varpi) \\ &\quad +\lambda'\tau(4+3\varpi+z_1\tau(5+2\varpi))+\lambda'^2(1+\varpi+z_1\tau(1+2\varpi))) \\ \delta_3 &= e^{z_2\tau+\varpi}z_1\tau(-\lambda'-2\tau)+e^{z_2\tau-\varpi}((\lambda'-2\tau)\varpi-z_2\tau(2\tau+\lambda'(1+2\varpi))) \\ \delta_4 &= e^{-z_1\tau-\varpi}z_2\tau(-\lambda'+2\tau)+e^{-z_1\tau+\varpi}((\lambda'+2\tau)\varpi+z_1\tau(2\tau+\lambda'(-1+2\varpi))) \end{aligned}\right\}, \tag{B11}$$

$$\left.\begin{aligned}
\delta_5 &= e^{-z_2\tau-\varpi}(-\lambda'+2\tau)(\lambda'(1-z_1\tau)+\tau(-2+z_1\tau))+e^{-z_2\tau+\varpi}(2\tau^2(2+z_2\tau+\varpi)\\
&\quad+\lambda'\tau(4+3\varpi+z_2\tau(5+2\varpi))+\lambda'^2(1+\varpi+z_2\tau(1+2\varpi)))\\
\delta_6 &= e^{z_1\tau+\varpi}(\lambda'+2\tau)(\lambda'(-1-z_2\tau)+\tau(-2-z_2\tau))+e^{z_1\tau-\varpi}(-2\tau^2(-2+z_1\tau+\varpi)\\
&\quad+\lambda'\tau(-4+3\varpi+z_1\tau(5-2\varpi))+\lambda'^2(1-\varpi+z_1\tau(-1+2\varpi)))\\
\delta_7 &= e^{-z_2\tau-\varpi}(\lambda'-2\tau)(z_2\tau-\varpi)+e^{-z_2\tau+\varpi}((\lambda'+2\tau)\varpi+z_2\tau(2\tau+(-1+2\varpi)\lambda'))\\
\delta_8 &= e^{z_1\tau+\varpi}(\lambda'+2\tau)(z_1\tau-\varpi)+e^{z_1\tau-\varpi}((\lambda'-2\tau)\varpi-z_1\tau(2\tau+(1+2\varpi)\lambda'))
\end{aligned}\right\}, \tag{B12}$$

$$\left.\begin{aligned}
\delta_9 &= e^{z_2\tau+\varpi}(\lambda'+2\tau)(-\lambda'-\tau)+e^{z_2\tau-\varpi}(\lambda'^2-5\lambda'\tau+2\tau^2+2\lambda'(-\lambda'+\tau)\varpi)\\
\delta_{10} &= e^{-z_1\tau-\varpi}(\lambda'-2\tau)(-\lambda'+\tau)+e^{-z_1\tau+\varpi}(\lambda'^2+5\lambda'\tau+2\tau^2+2\lambda'(\lambda'+\tau)\varpi)\\
\delta_{11} &= e^{z_2\tau+\varpi}(-\lambda'-2\tau)+e^{z_2\tau-\varpi}(2\tau+\lambda'(2\varpi+1))\\
\delta_{12} &= e^{-z_1\tau-\varpi}(\lambda'-2\tau)+e^{-z_1\tau+\varpi}(2\tau+\lambda'(2\varpi-1))
\end{aligned}\right\}, \tag{B13}$$

$$\left.\begin{aligned}
\delta_{13} &= e^{-z_2\tau-\varpi}(\lambda'-2\tau)(\lambda'-\tau)+e^{-z_2\tau+\varpi}(-2\tau^2-\lambda'((5+2\varpi)\tau+\lambda'(1+2\varpi)))\\
\delta_{14} &= e^{\varpi+z_1\tau}(\lambda'+2\tau)(\lambda'+\tau)+e^{z_1\tau-\varpi}(-2\tau^2+\lambda'((5-2\varpi)\tau+\lambda'(-1+2\varpi)))\\
\delta_{15} &= e^{-\varpi-z_2\tau}(2\tau-\lambda')+e^{\varpi-z_2\tau}(-2\tau+(1-2\varpi)\lambda')\\
\delta_{16} &= e^{\varpi+z_1\tau}(2\tau+\lambda')+e^{-\varpi+z_1\tau}(-2\tau-(1+2\varpi)\lambda')
\end{aligned}\right\}, \tag{B14}$$

$$\left.\begin{aligned}
b^*_{1n} &= \int_0^\infty L_1(\tau,z)\tau J_1(\tau\rho)d\tau, \quad d^*_{1n} = \int_0^\infty L_2(\tau,z)\tau J_1(\tau\rho)d\tau\\
b^*_{2n} &= \int_0^\infty M_1(\tau,z)\tau J_0(\tau\rho)d\tau, \quad d^*_{2n} = \int_0^\infty M_2(\tau,z)\tau J_0(\tau\rho)d\tau
\end{aligned}\right\}, \tag{B15}$$

$$\left.\begin{aligned}
L_1(\tau,z) &= (-B^*_{1n}e^{-\tau z}+B^*_{2n}e^{\tau z}+B^*_{3n}(1-\tau z)e^{-\tau z}+B^*_{4n}(1+z\tau)e^{\tau z})\\
L_2(\tau,z) &= (-D^*_{1n}e^{-\tau z}+D^*_{2n}e^{\tau z}+D^*_{3n}(1-\tau z)e^{-\tau z}+D^*_{4n}(1+z\tau)e^{\tau z})\\
M_1(\tau,z) &= -(B^*_{1n}e^{-\tau z}+B^*_{2n}e^{\tau z}+B^*_{3n}\tau z e^{-\tau z}+B^*_{4n}\tau z e^{\tau z})\\
M_2(\tau,z) &= -(D^*_{1n}e^{-\tau z}+D^*_{2n}e^{\tau z}+D^*_{3n}\tau z e^{-\tau z}+D^*_{4n}\tau z e^{\tau z})
\end{aligned}\right\}, \tag{B16}$$

$$\left.\begin{aligned}
B_{3n} &= r^{-n-2}(n^2-1)G_n(\zeta)\csc\theta\\
D_{3n} &= r^{-n}(n(n-2))G_n(\zeta)\csc\theta
\end{aligned}\right\}, \tag{B17}$$

$$\begin{aligned}
b^*_{3n} &= \frac{1}{r^2}\int_0^\infty (2\rho z\,\tau^2 J_0(\tau\rho)-(z+\tau(z^2-\rho^2))\tau J_1(\tau\rho))L_1(\tau,z)d\tau\\
&\quad+\frac{1}{r^2}\int_0^\infty (2(B^*_{2n}+(1+\tau z)B^*_{4n})(z^2-\rho^2)e^{\tau\,z}\tau^2 J_1(\tau\rho))d\tau,
\end{aligned} \tag{B18}$$

$$d_{3n}^{*} = \frac{1}{r^2}\int_0^\infty 2(D_{2n}^{*} + (1+\tau z)D_{4n}^{*})(z^2-\rho^2)e^{\tau z}\tau^2 J_1(\tau\rho)d\tau$$
$$+ \frac{1}{r^2}\int_0^\infty (2\rho z\,\tau^2 J_0(\tau\rho) - (z+\tau(z^2-\rho^2))\tau J_1(\tau\rho))L_2(\tau,z)d\tau. \quad \text{(B19)}$$

[1] J. Tyndall, Dust and disease, Fraser's Mag. **1.3**, 302 (1870).

[2] S. K. Friedlander, *Smoke, Dust, and Haze: Fundamentals of Aerosol Behaviour* (Wiley-Interscience, New York, 1977).

[3] A. G. B. M. Sasse, W. W. Nazaroff, and A. J. Gadgil, Particle filter based on thermophoretic deposition from natural convection flow, Aerosol Sci. Technol. **20**, 227 (1994).

[4] N. Montassier, D. Boulaud, and A. Renoux, Experimental study of thermophoretic particle deposition in laminar tube flow, J. Aerosol Sci. **22**, 677 (1991).

[5] M. C. Weinberg, Thermophoretic efficiency in modified chemical vapor deposition process, J. Am. Ceram. Soc. **65**, 81 (1982).

[6] Y. Ye, D. Y. H. Pui, B. Y. H. Liu, S. Opiolka, S. Blumhorst, and H. Fissan, Thermophoretic effect of particle deposition on a free-standing semiconductor wafer in a clean room, J. Aerosol Sci. **22**, 63 (1991).

[7] M. M. R. Williams, and S. K. Loyalka, *Aerosol Science: Theory and Practice with Special Applications to the Nuclear Industry* (Pergamon Press, New York, 1991).

[8] N. P. Balsara, and R. S. Subramanian, The influence of buoyancy on thermophoretic deposition of aerosol particles in a horizontal tube, J. Colloid Interface Sci. **118**, 3 (1987).

[9] A. Guha and S. Samanta, Effect of thermophoresis and its mathematical models on the transport and deposition of aerosol particles in natural convective flow on vertical and horizontal plates, J. Aerosol Sci. **77**, 85 (2014).

[10] A. Messerer, R. Niessner, and U. Poschl, Miniature pipe bundle heat exchanger for thermophoretic deposition of ultrafine soot aerosol particles at high flow velocities, Aerosol Sci. Technol. **38**, 456 (2004).

[11] B. Sagot, Thermophoresis for spherical particles, J. Aerosol Sci. **65**, 10 (2013).

[12] Y. T. Wu, B. Yang, and Y. Zhao, Thermophoresis of aerosol particles in near-critical vapor: An inverse size effect, Appl. Phys. Lett. **106**, 251605 (2015).

[13] A. Beskok and G. Karniadakis, *Microflows and Nanoflows: Fundamentals and Simulation*, Interdisciplinary Applied Mathematics (Springer, New York, 2005).

[14] C. Shen, *Rarefied Gas Dynamics: Fundamentals, Simulations, and Micro Flows* (Springer Science and Business Media, Berlin, 2006).

[15] J. R. Brock, On the theory of thermal forces acting on aerosol particles, J. Colloid Sci. **17**, 768 (1962).

[16] L. D. Reed, Low Knudsen number photophoresis, J. Aerosol Sci. **8**, 123 (1977).

[17] D. W. Mackowski, Photophoresis of aerosol particles in the free molecular and slip-flow regimes, Int. J. Heat Mass Transf. **32**, 843 (1989).

[18] S. K. Loyalka, Thermophoretic force on a single particle-I. Numerical solution of the linearized Boltzmann equation, J. Aerosol Sci. **23**, 291 (1992).

[19] S. Fayolle, T. Bickel, and A. Würger, Thermophoresis of charged colloidal particles, Phys. Rev. E **77**, 041404 (2008).

[20] J. Morthomas and A. Würger, Thermophoresis at a charged surface: the role of hydrodynamic slip, J. Phys.: Condens. Matter **21**, 035103 (2009).

[21] A. Würger, Thermally driven Marangoni Surfers, J. Fluid Mech. **752**, 589 (2014).

[22] A. Ly and A. Würger, Hydrodynamic interactions in DNA thermophoresis, Soft Matter **14**, 848 (2018).

[23] S. Duhr, S. Arduini, and D. Braun, Thermophoresis of DNA determined by microfluidic fluorescence, Eur. Phys. J. E **15**, 277 (2004).

[24] A. Parola and R. Piazza, Particle thermophoresis in liquids, Eur. Phys. J. E **15**, 255 (2004).

[25] J. C. Padrino, J. E. Sprittles, and D. A. Lockerby, Thermophoresis of a spherical particle: Modelling through moment-based, macroscopic transport equations, J. Fluid Mech. **862**, 312 (2019).
[26] S. Iacopini and R. Piazza, Thermophoresis in protein solutions, Europhys. Lett. **63**, 247 (2003).
[27] S. Duhr and D. Braun, Two-dimensional colloidal crystals formed by thermophoresis and convection, Appl. Phys. Lett. **86**, 131921 (2005).
[28] F. M. Weinert and D. Braun, Observation of Slip Flow in Thermophoresis, Phys. Rev. Lett. **101**, 168301 (2008).
[29] R. Piazza and A. Parola, Thermophoresis in colloidal suspensions, J. Phys.: Condens. Matter **20**, 153102 (2008).
[30] K. A. Eslahian, A. Majee, M. Maskos, and A.Würger, Specific salt effects on thermophoresis of charged colloids, Soft Matter **10**, 1931 (2014).
[31] J. Burelbach, D. Frenkel, I. Pagonabarraga, and E. Eiser, A unified description of colloidal thermophoresis, Eur. Phys. J. E **41**, 7 (2018).
[32] J. Burelbach, D. B. Brückner, D. Frenkel, and E. Eiser, Thermophoretic forces on a mesoscopic scale, Soft Matter **14**, 7446 (2018).
[33] S. Shakib, B. Rogez, S. Khadir, J. Polleux, A. Würger, and G. Baffou, Microscale thermophoresis in liquids induced by plasmonic heating and characterized by phase and fluorescence microscopies, J. Phys. Chem. C **125**, 21533 (2021).
[34] Y. Sone, Flow induced by a thermal stress in a rarefied gas, Phys. Fluids **15**, 1418 (1972).
[35] J. C. Maxwell, On stresses in rarefied gases arising from inequalities of temperature, Philos. Trans. R. Soc. **170**, 231 (1879).
[36] S. P. Bakanov, The nature of thermophoresis of highly heat-conducting bodies in gases, J. Appl. Math. Mech. **68**, 25 (2004).
[37] W. K. Li, C. Y. Soong, C. H. Liu, and P. Y. Tzeng, Thermophoresis of a micro-particle in gaseous media with effect of thermal stress slip, Aerosol Sci. Technol. **44**, 1077 (2010).
[38] Y. C. Chang and H. J. Keh, Effects of thermal stress slip on thermophoresis and photophoresis, J. Aerosol Sci. **50**, 1 (2012).
[39] E. I. Saad and M. S. Faltas, Theory of thermophoresis of a spherical particle embedded in a micropolar fluid, J. Mol. Liq. **282**, 527 (2019).
[40] M. S. Faltas and K. E. Ragab, Thermophoretic and photophoretic velocities and forces of a spherical particle embedded in Brinkman medium, Eur. Phys. J. Plus **134**, 475 (2019).
[41] M. S. Faltas and K. E. Ragab, Thermophoresis of cylindrical particle immersed in Brinkman fluid, Colloid J. **83**, 676 (2021).
[42] H. J. Keh and Y. C. Chang, Thermophoresis of an aerosol sphere perpendicular to two plane walls, AIChE J. **52**, 1690 (2006).
[43] S. Y. Lu and C. T. Lee, Thermophoretic motion of an aerosol particle in a non-concentric pore, J. Aerosol Sci. **32**, 1341 (2001).
[44] S. Y. Lu and C. T. Lee, Thermophoretic motion of a spherical aerosol particle in a cylindrical pore, Aerosol Sci. Technol. **37**, 455 (2003).
[45] H. H. Sherief, M. S. Faltas, and K. E. Ragab, Exact solution for the slow motion of a spherical particle in the presence of an interface with slip regime, Eur. Phys. J. Plus **136**, 466 (2021).
[46] H. H. Sherief, M. S. Faltas, and K. E. Ragab, Motion of a slip spherical particle near a planar micropolar-viscous interface, Eur. J. Mech. B Fluids **89**, 274 (2021).
[47] M. E. O'Neill and B. S. Bhatt, Slow motion of a solid sphere in the presence of a naturally permeable surface, Q. J. Mech. Appl. Math. **44**, 91 (1991).
[48] A. Würger, Hydrodynamic Boundary Effects on Thermophoresis of Confined Colloids, Phys. Rev. Lett. **116**, 138302 (2016).
[49] E. R. Damiano, D. S. Long, F. H. El-Khatib, and T. M. Stace, On the motion of a sphere in a Stokes flow parallel to a Brinkman half-space, J. Fluid Mech. **500**, 75 (2004).
[50] M. S. Faltas, H. H. Sherief, A. A. Allam, and B. A. Ahmed, Axisymmetric motion of a slip spherical particle in the presence of a Brinkman interface with stress jump, Eur. J. Mech. B Fluids **90**, 73 (2021).

[51] H. C. Brinkman, A calculation of the viscous force exerted by a flowing fluid on a dense swarm of particles, Flow Turbul. Combust. **1**, 27 (1949).
[52] J. A. Ochoa-Tapia and S. Whitaker, Momentum transfer at the boundary between a porous medium and a homogeneous fluid-I. Theoretical development, Int. J. Heat Mass Transfer **38**, 2635 (1995).
[53] F. J. Valdés-Parada, J. Alvarez-Ramírez, B. Goyeau, and J. A. Ochoa-Tapia, Computation of jump coefficients for momentum transfer between a porous medium and a fluid using a closed generalized transfer equation, Transp. Porous Media **78**, 439 (2009).
[54] J. Happel and H. Brenner, *Low Reynolds Number Hydrodynamics: With Special Applications to Particulate Media* (Springer Science and Business Media, New York, 2012).
[55] Y. C. Chang and H. J. Keh, Thermophoresis at small but finite Péclet numbers, Aerosol Sci. Technol. **52**, 1028 (2018).
[56] G. S. Beavers and D. D. Joseph, Boundary conditions at a naturally permeable wall, J. Fluid Mech. **30**, 197 (1967).
[57] P. Saffman, On the boundary condition at the surface of a porous medium, MIT Stud. Appl. Math. **50**, 93 (1971).
[58] F. Sharipov and D. Kalempa, Velocity slip and temperature jump coefficients for gaseous mixtures. IV. Temperature jump coefficient, Int. J. Heat Mass Transf. **48**, 1076 (2005).
[59] J. B. Young, Thermophoresis of a spherical particle: reassessment, clarification, and new analysis, Aerosol Sci. Technol. **45**, 927 (2011).
[60] S. El-Sapa and M. S. Faltas, Mobilities of two spherical particles immersed in a magneto-micropolar fluid, Phys. Fluids **34**, 013104 (2022).
[61] P. Ganatos, S. Weinbaum, and R. Pfeffer, A strong interaction theory for the creeping motion of a sphere between plane parallel boundaries. Part 1. Perpendicular motion J. Fluid Mech. **99**, 739 (1980).
[62] L. Talbot, R. K. Cheng, R. W. Schefer, and D. R. Willis, Thermophoresis of particles in heated boundary layer, J. Fluid Mech. **101**, 737 (1980).
[63] D. A. Lockerby, J. M. Reese, D. R. Emerson, and R. W. Barber, Velocity boundary condition at solid walls in rarefied gas calculations, Phys. Rev. E **70**, 017303 (2004).
[64] C. Y. Soong, W. K. Li, C. H. Liu, and P. Y. Tzeng, Effect of thermal stress slip on microparticle photophoresis in gaseous media, Opt. Lett. **35**, 625 (2010).
[65] D. P. Shoemaker, C. W. Garland, J. I. Steinfeld, and J. W. Nibler, *Experiments in Physical Chemistry*, 4th ed. (McGraw-Hill, New York, 1981).
[66] M. Yang and M. Ripoll, Thermophoretically induced flow field around a colloidal particle, Soft Matter **9**, 4661 (2013).